

Fitted Value Iteration Methods for Bicausal Optimal Transport

Erhan Bayraktar
Department of Mathematics
University of Michigan
Ann Arbor, MI 48109-1043, USA

ERHAN@UMICH.EDU

Bingyan Han
Department of Mathematics
University of Michigan
Ann Arbor, MI 48109-1043, USA

BYHAN@UMICH.EDU

Abstract

We develop a fitted value iteration (FVI) method to compute bicausal optimal transport (OT) where couplings have an adapted structure. Based on the dynamic programming formulation, FVI adopts a function class to approximate the value functions in bicausal OT. Under the concentrability condition and approximate completeness assumption, we prove the sample complexity using (local) Rademacher complexity. Furthermore, we demonstrate that multilayer neural networks with appropriate structures satisfy the crucial assumptions required in sample complexity proofs. Numerical experiments reveal that FVI outperforms linear programming and adapted Sinkhorn methods in scalability as the time horizon increases, while still maintaining acceptable accuracy.

Keywords: Bicausal optimal transport, fitted value iteration, Rademacher complexity, covering number, multilayer neural networks

1 Introduction

Optimal transport (OT) has emerged as a valuable tool for comparing probability distributions, finding applications in diverse disciplines such as mathematics, statistics, machine learning, and economics. OT possesses an intuitive geometric interpretation, quantifying the costs involved in transforming one probability distribution into another by moving point masses. Although the concept of OT originated in the works of Monge in 1781 and Kantorovich in the 1940s (Villani, 2009, Chapter 3), its widespread adoption was catalyzed by the development of an efficient computational method utilizing entropic regularization, known as the Sinkhorn algorithm (Cuturi, 2013). These advancements have alleviated the computational burden associated with OT, contributing to its increased popularity.

Temporal data play a ubiquitous role in various domains, such as finance (e.g., stock prices) and computer science (e.g., videos) (Xu et al., 2020). However, the conventional OT framework fails to account for the temporal structure and information flow inherent in such data. To address this limitation, a recent surge of research introduced causal OT with a non-anticipative framework (Lassalle, 2013; Backhoff-Veraguas et al., 2017). In essence, causal OT requires that when the past of one process, X , is given, the past of another process, Y , should be independent of the future of X under the transport plan. If the same condition holds after interchanging the role of X and Y , the transport plan is called

bicausal; see Pflug and Pichler (2012); Acciaio et al. (2020); Backhoff-Veraguas et al. (2020); Xu et al. (2020); Acciaio et al. (2021) for recent applications.

The classical OT method is hindered by its high computational costs, and the inclusion of the temporal dimension in causal OT further exacerbates the computational challenges. Addressing this issue, Eckstein and Pammer (2023) recently proposed an adapted Sinkhorn algorithm tailored specifically for causal OT, based on the Bregman iterative formulation of the Sinkhorn algorithm (Peyré and Cuturi, 2019, Remark 4.8). As with previous approaches, continuous distributions are approximated using either empirical samples or quantization techniques. However, it is important to note that even the classical Sinkhorn algorithm requires $O(N^2)$ operations for a sample size of N (Genevay et al., 2019), which may not scale well under large sample sizes, particularly in high-dimensional scenarios. Furthermore, the adapted Sinkhorn algorithm in Eckstein and Pammer (2023, Lemma 6.4) enumerates all possible scenarios at each time step, and this enumeration grows rapidly as the time horizon increases.

The computational burden arising from discretization is not unique to OT, but rather a common challenge also encountered in dynamic programming (DP) applications, such as vehicle routing, healthcare, and energy optimization (Powell, 2007). Discretization often leads to an immense number of states, rendering the Bellman equation computationally intractable. To address this issue, approximate DP and reinforcement learning (RL) techniques have been developed to provide approximations of value functions or optimal policies. The use of neural networks as function approximators for action-value functions enables handling tasks with high-dimensional inputs (Mnih et al., 2015). It is worth noting that discretization approaches often neglect the structural properties inherent in value functions and optimal policies. For example, under certain conditions, the Wasserstein distance $W_p(\mu(dx_{1:T}|x'_0), \nu(dy_{1:T}|y'_0))$ between two conditional distributions $\mu(dx_{1:T}|x'_0)$ and $\nu(dy_{1:T}|y'_0)$ should not vary too much compared with $W_p(\mu(dx_{1:T}|x_0), \nu(dy_{1:T}|y_0))$, where (x'_0, y'_0) is close to (x_0, y_0) . Knowledge about $W_p(\mu(dx_{1:T}|x_0), \nu(dy_{1:T}|y_0))$ can be beneficial in determining $W_p(\mu(dx_{1:T}|x'_0), \nu(dy_{1:T}|y'_0))$.

Function approximators have also been utilized in the computation of OT, primarily as potential functions in the dual formulation, as discussed in Genevay et al. (2016); Seguy et al. (2018); Korotin et al. (2021). Notably, bicausal OT can be solved by DP (Backhoff-Veraguas et al., 2017, Corollary 3.3), which opens up possibilities for leveraging RL methods. In this regard, transport plans serve as control policies. In our work, we employ the fitted value iteration (FVI) technique from offline RL (Gordon, 1999; Munos and Szepesvári, 2008; Duan et al., 2021), which also eliminates the need for knowing the underlying distributions. In contrast to prior research, we utilize neural networks as approximators for the value functions in the primal formulation. Consequently, we derive the following theoretical and numerical results:

To analyze the sample complexity and error bounds of FVI, we adopt the concentrability condition introduced in Munos (2003); Munos and Szepesvári (2008); Duan et al. (2021); Fan et al. (2020); Chen and Jiang (2019) to establish a connection between value suboptimality and Bellman errors in Lemma 3. Leveraging standard tools in (local) Rademacher complexity (Mohri et al., 2018; Bartlett et al., 2005) and the convergence of empirical measures in Wasserstein distance (Fournier and Guillin, 2015; Genevay et al., 2019), we derive the sample complexity for FVI in Theorems 10 and 16 and Corollaries 11 and 17. Addi-

tionally, to demonstrate the feasibility of the crucial approximate completeness assumption 6 and the specific Lipschitz assumption 7, we establish that neural networks with rectified linear unit (ReLU) and sigmoid activation functions satisfy these assumptions when appropriately structured. Notably, recent advancements in approximating Hölder functions with neural networks in Schmidt-Hieber (2020); Langer (2021) provide explicit bounds on the approximate completeness assumption 6. Moreover, the fixed point of a sub-root function in Assumption 14 can be bounded on the order of $\ln(N)/N$ using the covering number technique.

Numerically, we conducted a comparison between FVI and linear programming (LP) and adapted Sinkhorn algorithms. With Gaussian data, we observed that the LP and adapted Sinkhorn methods provided highly accurate estimates with low variances. Additionally, these methods demonstrated faster convergence than FVI for short time horizons. However, as the time horizon increased, FVI exhibited superior scalability compared to the LP and adapted Sinkhorn methods. Notably, for time horizons $T \geq 20$, the LP and adapted Sinkhorn methods failed to converge within a reasonable time frame, while FVI obtained estimations with satisfactory accuracy. Moreover, our implementation offered a unified approach to handling multidimensional data.

The structure of this paper is as follows: Section 1.1 and Section 1.2 introduce the notation and bicausal OT, respectively. Section 2 presents the FVI algorithm for bicausal OT, while Section 3 provides the proof of sample complexity. In Section 4, we demonstrate that the ReLU and sigmoid neural networks satisfy crucial assumptions outlined in Section 3. We present the numerical comparison in Section 5. Our code is available at <https://github.com/hanbingyan/FVIOT>. The Appendix summarizes auxiliary results used in the proof.

1.1 Notation and Preliminaries

We summarize frequently used notations here. Denote $\lceil x \rceil$ as the least integer greater than or equal to x . For two numbers a and b , let $a \vee b = \max\{a, b\}$. For a function $f : \mathcal{S} \rightarrow \mathbb{R}$, $\|f\|_\infty := \sup_{s \in \mathcal{S}} |f(s)|$ is the uniform norm. Denote $\|W\|_\infty$ as the maximum-entry norm of a vector or matrix W . Denote $\|W\|_0$ as the number of non-zero entries of W . For two real-valued functions $f(\cdot)$ and $g(\cdot)$, we write $f(\cdot) \lesssim g(\cdot)$ if $f(\cdot) \leq C \cdot g(\cdot)$ with an absolute constant C independent of function parameters. Denote \mathcal{C}^∞ as the set of infinitely differentiable functions.

Let a positive integer T be the finite number of periods. For each $t \in \{0, 1, \dots, T-1, T\}$, suppose \mathcal{X}_t is a closed subset of \mathbb{R}^d . \mathcal{X}_t stands for the range of the process at time t . $\mathcal{X} := \mathcal{X}_{0:T} = \mathcal{X}_0 \times \dots \times \mathcal{X}_T$ is a closed subset of $\mathbb{R}^{(T+1) \times d}$. Denote the set of all Borel probability measures on \mathcal{X} as $\mathcal{P}(\mathcal{X})$. We write $\mu(dx_{t+1:T}|x_{0:t})$ as the regular conditional probability kernel of $x_{t+1:T}$ given $x_{0:t}$, which is uniquely determined in a suitable way (Bogachev, 2007, Theorem 10.4.14 and Corollary 10.4.17).

With a fixed $p \in [1, \infty)$, we introduce the metric as $d_{\mathcal{X}}(x_{0:T}, x'_{0:T}) = \left[\sum_{t=0}^T |x_t - x'_t|^p \right]^{1/p}$ for $x, x' \in \mathcal{X}$ and equip \mathcal{X} with the corresponding Polish topology. The Wasserstein space of order p is given by

$$\mathcal{P}_p(\mathcal{X}) := \left\{ \mu \in \mathcal{P}(\mathcal{X}) \mid \int_{\mathcal{X}} d_{\mathcal{X}}(x_{0:T}, \bar{x}_{0:T})^p \mu(dx) < \infty \right\}$$

for some fixed $\bar{x}_{0:T} \in \mathcal{X}$.

The Wasserstein distance has been widely used as a metric on probability spaces. Consider two Borel probability measures $\mu, \mu' \in \mathcal{P}(\mathcal{X})$. A coupling $\gamma \in \mathcal{P}(\mathcal{X} \times \mathcal{X})$ is a Borel probability measure that admits μ and μ' as its marginals on \mathcal{X} . Denote $\Pi(\mu, \mu')$ as the set of all the couplings. The Wasserstein distance of order p between μ and μ' is given by

$$W_p(\mu, \mu') = \left(\inf_{\gamma \in \Pi(\mu, \mu')} \int_{\mathcal{X} \times \mathcal{X}} d_{\mathcal{X}}(x, x')^p \gamma(dx, dx') \right)^{1/p}. \quad (1)$$

We introduce another closed set $\mathcal{Y} = \mathcal{Y}_{0:T} = \mathcal{Y}_0 \times \dots \times \mathcal{Y}_T$ similarly. Denote a metric on \mathcal{Y} as $d_{\mathcal{Y}}(y_{0:T}, y'_{0:T}) = \left[\sum_{t=0}^T |y_t - y'_t|^p \right]^{1/p}$ for $y, y' \in \mathcal{Y}$ and equip \mathcal{Y} with the corresponding Polish topology. Under the metric $d_{\mathcal{Y}}$, we introduce $\mathcal{P}_p(\mathcal{Y})$ as the Wasserstein space of order p and $W_p(\nu, \nu')$ as the Wasserstein metric on $\mathcal{P}_p(\mathcal{Y})$.

For the product space $\mathcal{X} \times \mathcal{Y}$, we define the corresponding Wasserstein space of order p as

$$\mathcal{P}_p(\mathcal{X} \times \mathcal{Y}) := \left\{ \pi \in \mathcal{P}(\mathcal{X} \times \mathcal{Y}) \mid \int_{\mathcal{X} \times \mathcal{Y}} d((x, y), (\bar{x}, \bar{y}))^p \pi(dx, dy) < \infty \right\},$$

with the metric d given by

$$d((x, y), (\bar{x}, \bar{y})) = [d_{\mathcal{X}}(x, \bar{x})^p + d_{\mathcal{Y}}(y, \bar{y})^p]^{1/p}.$$

For two probability measures $\pi, \pi' \in \mathcal{P}_p(\mathcal{X} \times \mathcal{Y})$, the Wasserstein distance between them is denoted by

$$W_p(\pi, \pi') = \left(\inf_{\gamma \in \Pi(\pi, \pi')} \int_{\mathcal{X} \times \mathcal{Y} \times \mathcal{X} \times \mathcal{Y}} d((x, y), (x', y'))^p \gamma(dx, dy, dx', dy') \right)^{1/p}.$$

1.2 Bicausal Optimal Transport

Consider two probability measures $\mu \in \mathcal{P}(\mathcal{X})$ and $\nu \in \mathcal{P}(\mathcal{Y})$. Recall $\Pi(\mu, \nu)$ is the set of all the couplings that admit μ and ν as marginals. Suppose transporting one unit of mass from x to y incurs a cost of $c(x, y)$. A generic OT problem is formulated as

$$\mathcal{W}(\mu, \nu) := \inf_{\pi \in \Pi(\mu, \nu)} \int_{\mathcal{X} \times \mathcal{Y}} c(x, y) \pi(dx, dy),$$

with the Wasserstein distance of order p in (1) as a special case.

If the data have a temporal structure as $x = (x_0, \dots, x_t, \dots, x_T)$ and $y = (y_0, \dots, y_t, \dots, y_T)$, not all couplings $\pi \in \Pi(\mu, \nu)$ will make sense. A natural requirement of the transport plan $\pi(x, y)$ should be the non-anticipative condition. Informally speaking, if the past of x is given, then the past of y should be independent of the future of x under the measure π . Mathematically, it means a transport plan π should satisfy

$$\pi(dy_t | dx_{0:T}) = \pi(dy_t | dx_{0:t}), \quad t = 0, \dots, T-1, \quad \pi\text{-a.s.} \quad (2)$$

The property (2) is known as the causality condition and the transport plan satisfying (2) is called *causal* by Lassalle (2013). If the same condition holds when we exchange the

positions of x and y , then the transport plan is called bicausal. Denote $\Pi_{bc}(\mu, \nu)$ as the set of all bicausal transport plans between μ and ν . The bicausal OT problem considers the optimization over $\Pi_{bc}(\mu, \nu)$ only:

$$\mathcal{W}_{bc}(\mu, \nu) := \inf_{\pi \in \Pi_{bc}(\mu, \nu)} \int_{\mathcal{X} \times \mathcal{Y}} c(x, y) \pi(dx, dy). \quad (3)$$

For applications of causal and bicausal OT, see Backhoff-Veraguas et al. (2020); Xu et al. (2020); Acciaio et al. (2021); Pflug and Pichler (2012); Acciaio et al. (2020) for an incomplete list.

In this paper, we consider two probability measures μ and ν with symmetric positions and focus on the bicausal transport plans only. For a given transport plan $\pi \in \Pi(\mu, \nu)$, we can decompose π in terms of successive regular kernels:

$$\begin{aligned} \pi(dx_{0:T}, dy_{0:T}) = & \bar{\pi}(dx_0, dy_0) \pi(dx_1, dy_1 | x_0, y_0) \pi(dx_2, dy_2 | x_{0:1}, y_{0:1}) \dots \\ & \pi(dx_T, dy_T | x_{0:T-1}, y_{0:T-1}), \end{aligned} \quad (4)$$

which is uniquely determined in a suitable way (Bogachev, 2007, Theorem 10.4.14 and Corollary 10.4.17). By Backhoff-Veraguas et al. (2017, Proposition 5.1), π is a bicausal transport plan if and only if

- (1) $\bar{\pi} \in \Pi(p_*^1 \mu, p_*^1 \nu)$, and
- (2) for each $t = 0, \dots, T-1$ and π -almost every path $(x_{0:t}, y_{0:t})$, the following condition holds:

$$\pi(dx_{t+1}, dy_{t+1} | x_{0:t}, y_{0:t}) \in \Pi(\mu(dx_{t+1} | x_{0:t}), \nu(dy_{t+1} | y_{0:t})).$$

$p_*^1 \mu$ (resp. $p_*^1 \nu$) is the pushforward of μ (resp. ν) by the projection p^1 onto the first coordinate.

To ease the notation, we denote $s_t := (x_t, y_t)$ which is interpreted as the state in RL. We adopt the convention that $s_{0:t} = (x_{0:t}, y_{0:t})$. Denote $\mathcal{S} := \mathcal{X} \times \mathcal{Y}$ as the range of states. For the completion of notation, we interpret $\pi(ds_{1:0} | s_0) = \delta_{s_0}$ as the Dirac measure at s_0 . For simplicity, denote the set of couplings as $\Pi(\mu^t, \nu^t, s_{0:t}) := \Pi(\mu(dx_{t+1} | x_{0:t}), \nu(dy_{t+1} | y_{0:t}))$. With a given initial state s_0 and a cost function depending on $s_{1:T}$, we introduce the initial value function for bicausal OT (3) as

$$V_0(s_0) := \inf_{\pi \in \Pi_{bc}(\mu, \nu, s_0)} \int c(s_{1:T}) \pi(ds_{1:T} | s_0). \quad (5)$$

2 Fitted Value Iteration

2.1 Motivation

In line with the conventional OT framework, computational methods have been developed for bicausal OT, employing both primal and dual formulations. The inclusion of causality introduces a linear constraint on transport plans. The strong duality results for causal and bicausal OT were established by Backhoff-Veraguas et al. (2017, Theorem 2.6) and Backhoff-Veraguas et al. (2017, Corollary 3.3), respectively. For the discrete case of causal

OT, Acciaio et al. (2021, Algorithm 1) incorporated basis functions for causality testing and then employed the Sinkhorn algorithm, while for the continuous case, Xu et al. (2020) utilized neural networks to model the test functions instead. It is worth noting that the Sinkhorn algorithm can be interpreted as Bregman iterative projections (Peyré and Cuturi, 2019, Remark 4.8). With this observation, Eckstein and Pammer (2023) introduced an adapted version of the Sinkhorn algorithm. Besides, Pichler and Weinhardt (2022) also proposed a nested Sinkhorn algorithm. For the distinctions between these two methods, please refer to Eckstein and Pammer (2023, Remark 6.12). Finally, analogous to the classical OT, the LP formulation is also available for discrete causal and bicausal OT (Eckstein and Pammer, 2023, Lemma 3.11).

All these methods mainly handle discrete distributions or samples from continuous distributions. The LP and Sinkhorn algorithms require $O(N^3 \log N)$ and $O(N^2)$ operations respectively, based on a sample of size N (Genevay et al., 2019). However, even the Sinkhorn algorithm may encounter scalability issues when dealing with a large number of samples. Furthermore, the computational burden in causal and bicausal OT is exacerbated by the temporal dimension T . The adapted Sinkhorn algorithm discussed in Eckstein and Pammer (2023, Lemmas 6.2 and 6.6) necessitates iterating over all possible scenarios at each time t , with the number of scenarios rapidly growing as the time horizon increases. It's important to note that these challenges are not unique to causal and bicausal OT but also arise in other fields, including DP. A crucial observation is that for a good cost function c and marginals μ and ν , if two states s_0 and s'_0 are close, then the values $V_0(s_0)$ and $V_0(s'_0)$ defined in (5) should also be close. These structural properties are ignored when using matrices to model value functions.

Given the DP formulation for bicausal OT (6), we posit that techniques capable of addressing the computational challenges in DP may also find applicability in bicausal OT. As the state space can be vast, it often becomes necessary to employ approximation techniques. Approximate DP and RL frequently leverage specific functions to approximate the value functions or optimal policies. In this study, we employ FVI to compute the bicausal OT costs, drawing inspiration from its successful applications in Munos and Szepesvári (2008) and batch RL (Duan et al., 2021). FVI provides a unified approach for handling continuous distributions and high-dimensional data, exhibiting superior scalability compared to previous methods. Our FVI algorithm operates in the primal form, utilizing neural networks to approximate the value functions. In contrast, prior literature has utilized neural networks to model potential functions in the dual formulation (Genevay et al., 2016; Seguy et al., 2018; Korotin et al., 2021).

2.2 Algorithm

Backhoff-Veraguas et al. (2017) proved the DP principle for bicausal transport. Consider the recursive formulation

$$\begin{cases} V_t(s_{0:t}) = \inf_{\pi(ds_{t+1}|s_{0:t}) \in \Pi(\mu^t, \nu^t, s_{0:t})} \int V_{t+1}(s_{0:t}, s_{t+1}) \pi(ds_{t+1}|s_{0:t}), & t = 0, \dots, T-1, \\ V_T(s_{0:T}) = c(s_{1:T}). \end{cases} \quad (6)$$

By Backhoff-Veraguas et al. (2017, Proposition 5.2), if the cost function $c(s_{1:T})$ is lower semicontinuous and bounded from below, μ and ν are successively weakly continuous in the

sense that for each $t = 0, \dots, T - 1$,

$$x_{0:t} \mapsto \mu(dx_{t+1:T}|x_{0:t}) \text{ and } y_{0:t} \mapsto \mu(dy_{t+1:T}|y_{0:t})$$

are continuous with respect to the weak topologies on $\mathcal{P}(\mathcal{X})$ and $\mathcal{P}(\mathcal{Y})$. Then there is a bicausal optimizer and the recursive formulation (6) is well-defined. The value function V_t is lower semicontinuous. We will consider a continuous and bounded cost function in Assumption 5.

Algorithm 1 Fitted value iteration

- 1: **Input:** Sampling distribution β ; a fixed initial state s_0 ; initial neural network $f_t(s_{0:t})$, $t = 0, 1, \dots, T - 1$. Denote $f_T(s_{0:T}) = \hat{f}_T(s_{0:T}) = c(s_{1:T})$.
- 2: **for** $t = T - 1, T - 2, \dots, 0$ **do**
- 3: Sample a mini-batch of N paths $s_{0:t}^{n_t} = (x_{0:t}^{n_t}, y_{0:t}^{n_t})$, $n_t = 1, \dots, N$, according to $\beta(ds_{1:t}|s_0)$. Return s_0 when $t = 0$.
- 4: **for** $n_t = 1, \dots, N$ **do**
- 5: Construct empirical measures $\hat{\mu}_B(dx_{t+1}|x_{0:t}^{n_t})$ and $\hat{\nu}_B(dy_{t+1}|y_{0:t}^{n_t})$ with size B .
- 6: Calculate the empirical OT to approximate the value function at $s_{0:t}^{n_t}$:

$$\hat{V}_t(s_{0:t}^{n_t}) \leftarrow \inf_{\pi_t \in \Pi(\hat{\mu}_B^t, \hat{\nu}_B^t, s_{0:t}^{n_t})} \int \hat{f}_{t+1}(s_{0:t}^{n_t}, s_{t+1}) \pi_t(ds_{t+1}). \quad (7)$$

- 7: **end for**
- 8: Minimize the empirical loss by performing G gradient descent steps on parameters of f_t . Obtain

$$\hat{f}_t \leftarrow \arg \min_{f_t \in \mathcal{F}_t} \frac{1}{N} \sum_{n_t=1}^N \left(f_t(s_{0:t}^{n_t}) - \hat{V}_t(s_{0:t}^{n_t}) \right)^2. \quad (8)$$

- 9: **end for**
 - 10: **Output:** Value function approximators by neural network $\hat{f}_t(s_{0:t})$, $t = 0, 1, \dots, T - 1$.
-

Algorithm 1 for bicausal OT is inspired by FVI in RL (Munos and Szepesvári, 2008; Duan et al., 2021). To learn the true value function V_t , FVI adopts an approximator $f_t(s_{0:t}) \in \mathcal{F}_t$, where \mathcal{F}_t is certain function class. In particular, $f_T(s_{0:T}) := c(s_{1:T})$. Denote $f := (f_0, \dots, f_T)$ and $\mathcal{F} := \mathcal{F}_0 \times \dots \times \mathcal{F}_T$ with $\mathcal{F}_T := \{c(s_{1:T})\}$.

FVI visits states s according to a sampling distribution β . β should be able to obtain representative samples and exhaust all possible states in a certain sense, as outlined in Assumption 2. Given a state $s_{0:t}$, we use the empirical distribution to calculate an approximation $\hat{V}_t(s_{0:t})$ to the value function $V_t(s_{0:t})$ in (7). We denote the set of couplings between empirical measures by $\Pi(\hat{\mu}_B^t, \hat{\nu}_B^t, s_{0:t}) := \Pi(\hat{\mu}_B(dx_{t+1}|x_{0:t}), \hat{\nu}_B(dy_{t+1}|y_{0:t}))$, where constant B is the sample size. For notation convenience, we denote the Bellman operator as

$$\mathcal{T}[f_{t+1}](s_{0:t}) := \inf_{\pi(ds_{t+1}|s_{0:t}) \in \Pi(\mu^t, \nu^t, s_{0:t})} \int f_{t+1}(s_{0:t}, s_{t+1}) \pi(ds_{t+1}|s_{0:t}). \quad (9)$$

To approximate the value function at a given point, (7) uses the empirical measures for marginals. Then we denote the empirical Bellman operator as

$$\hat{\mathcal{T}}_B[f_{t+1}](s_{0:t}) := \inf_{\pi(ds_{t+1}|s_{0:t}) \in \Pi(\hat{\mu}_B^t, \hat{\nu}_B^t, s_{0:t})} \int f_{t+1}(s_{0:t}, s_{t+1}) \pi(ds_{t+1}|s_{0:t}). \quad (10)$$

When the mini-batch size B is large, the classical empirical OT problem in (7) incurs a high computational burden. Then we can consider entropic regularization and the Sinkhorn algorithm (Cuturi, 2013). Denote the regularization parameter as $\varepsilon > 0$. We replace (7) with

$$\begin{aligned} \hat{V}_{\varepsilon,t}(s_{0:t}^{n_t}) \leftarrow & \inf_{\pi_t \in \Pi(\hat{\mu}_B^t, \hat{\nu}_B^t, s_{0:t}^{n_t})} \int \hat{f}_{t+1}(s_{0:t}^{n_t}, s_{t+1}) \pi_t(ds_{t+1}) \\ & + \varepsilon \text{KL} \left(\pi(ds_{t+1}|s_{0:t}^{n_t}) \parallel \hat{\mu}_B(dx_{t+1}|x_{0:t}^{n_t}) \otimes \hat{\nu}_B(dy_{t+1}|y_{0:t}^{n_t}) \right). \end{aligned}$$

$\text{KL}(\mathbb{P} \parallel \mathbb{Q}) = \int \ln \left(\frac{d\mathbb{P}}{d\mathbb{Q}} \right) d\mathbb{P}$ stands for the Kullback–Leibler divergence. Correspondingly, $\hat{V}_t(s_{0:t}^{n_t})$ in Algorithm 1 is replaced by $\hat{V}_{\varepsilon,t}(s_{0:t}^{n_t})$.

For later use, when entropic regularization is adopted, we denote the entropic Bellman operator and the empirical counterpart as

$$\begin{aligned} \mathcal{T}_{\varepsilon}[f_{t+1}](s_{0:t}) &:= \inf_{\pi(ds_{t+1}|s_{0:t}) \in \Pi(\mu^t, \nu^t, s_{0:t})} \int f_{t+1}(s_{0:t}, s_{t+1}) \pi(ds_{t+1}|s_{0:t}) \\ &\quad + \varepsilon \text{KL} \left(\pi(ds_{t+1}|s_{0:t}) \parallel \mu(dx_{t+1}|x_{0:t}) \otimes \nu(dy_{t+1}|y_{0:t}) \right), \\ \hat{\mathcal{T}}_{\varepsilon,B}[f_{t+1}](s_{0:t}) &:= \inf_{\pi(ds_{t+1}|s_{0:t}) \in \Pi(\hat{\mu}_B^t, \hat{\nu}_B^t, s_{0:t})} \int f_{t+1}(s_{0:t}, s_{t+1}) \pi(ds_{t+1}|s_{0:t}) \\ &\quad + \varepsilon \text{KL} \left(\pi(ds_{t+1}|s_{0:t}) \parallel \hat{\mu}_B(dx_{t+1}|x_{0:t}) \otimes \hat{\nu}_B(dy_{t+1}|y_{0:t}) \right). \end{aligned}$$

To find an approximator \hat{f}_t of the value function V_t , we perform the empirical risk minimization (ERM) in (8) with the squared loss function. (8) uses the empirical estimation $\hat{V}_t(s_{0:t}^{n_t})$. The corresponding theoretical optimization problem for (8) is

$$\min_{f_t \in \mathcal{F}_t} \int (f_t(s_{0:t}) - \mathcal{T}[\hat{f}_{t+1}](s_{0:t}))^2 \beta(ds_{1:t}|s_0). \quad (11)$$

In this work, we always assume that the infima in (8) and (11) are attained. This assumption holds under relatively mild conditions, such as the compactness of \mathcal{F}_t with respect to the squared loss function. When we consider neural networks with parameters from compact domains, this assumption can be guaranteed. For later use, we denote the loss function as

$$\mathcal{L}(f_t(s_{0:t}), \mathcal{T}[f_{t+1}](s_{0:t})) := (f_t(s_{0:t}) - \mathcal{T}[f_{t+1}](s_{0:t}))^2. \quad (12)$$

FVI introduces several inevitable errors, especially with continuous marginals μ and ν . First, instead of utilizing the true sample distribution β in (8), we can only sample a finite number of states s^{n_t} . This introduces the error associated with ERM, which can be further decomposed into approximation error and estimation error, as discussed in Shalev-Shwartz and Ben-David (2014, Section 5.2). Second, the true value of $V(s_{0:t})$ is unknown and needs to be approximated by $\hat{V}_t(s_{0:t})$ in (7), which introduces additional errors. Third, ERM in (8) relies on optimization methods like gradient descent to find an optimizer \hat{f}_t . However, the optimization algorithm may not converge to the exact optimizer and is typically terminated when a certain level of accuracy is reached. Consequently, this introduces optimization

errors (Bottou and Bousquet, 2007, Section 2.2). In this work, we always assume the optimizer in the ERM (8) can be obtained and thus ignore the optimization error. The FVI algorithm proceeds in a backward manner, and these errors propagate along the time dimension. In Section 3, we delve into the analysis of sample complexity and establish error bounds.

3 Sample Complexity

3.1 Value Suboptimality and Bellman Error

To evaluate the performance of FVI, we introduce the objective functional for a bicausal transport plan π as follows:

$$J_0(s_0; \pi) := \int c(s_{1:T}) \pi(ds_{1:T} | s_0). \quad (13)$$

Denote the optimal bicausal transport plan as π^* . Given an approximator $f = (f_0, \dots, f_T)$, we denote π^f as a transport plan implied by f . In other words, π^f is obtained by

$$\pi^f(ds_{t+1} | s_{0:t}) \in \arg \min_{\pi(ds_{t+1} | s_{0:t}) \in \Pi(\mu^t, \nu^t, s_{0:t})} \int f_{t+1}(s_{0:t}, s_{t+1}) \pi(ds_{t+1} | s_{0:t}). \quad (14)$$

Definition 1 introduces the concept of value suboptimality to measure the accuracy of an approximator f .

Definition 1 *Given an initial state s_0 , an approximator f is said to be ε -optimal if*

$$2 \left| f_0(s_0) - \int f_1(s_{0:1}) \pi^f(ds_1 | s_0) \right| + J_0(s_0; \pi^f) - J_0(s_0; \pi^*) \leq \varepsilon.$$

Our definition of ε -optimality differs slightly from its counterpart in RL (Duan et al., 2021, Definition 2.1). In our case, π^f depends only on (f_1, \dots, f_T) and not on f_0 . Therefore, we include the first term to account for the suboptimality of f_0 in Definition 1. The constant 2 is introduced for scaling purposes.

Value suboptimality in Definition 1 can be bounded by another surrogate criterion known as the Bellman error, which is defined as follows:

$$\mathcal{B}(f) := (f_0(s_0) - \mathcal{T}[f_1](s_0))^2 + \sum_{t=1}^{T-1} \int (f_t(s_{0:t}) - \mathcal{T}[f_{t+1}](s_{0:t}))^2 \beta(ds_{1:t} | s_0). \quad (15)$$

To establish their relationship, we introduce the concentrability coefficient (Munos, 2003) as follows:

Assumption 2 *Given an initial state s_0 , for any time $t = 0, \dots, T-1$ and bicausal transport $\pi(ds_{1:t} | s_0)$, suppose there exists a constant $C \geq 1$ such that*

$$\int_{\mathcal{X}_{1:t} \times \mathcal{Y}_{1:t}} \left(\frac{\pi(ds_{1:t} | s_0)}{\beta(ds_{1:t} | s_0)} \right)^2 \beta(ds_{1:t} | s_0) \leq C.$$

The $t = 0$ case is interpreted as Dirac measures.

The concentrability coefficient is widely used in RL with Markov decision processes (MDPs); see Munos (2003, Equation 7), Munos and Szepesvári (2008, Assumption A.2), Fan et al. (2020); Duan et al. (2021); Nguyen-Tang et al. (2022). Munos and Szepesvári (2008) compared it with the top-Lyapunov exponent of the MDP. Chen and Jiang (2019, Section 4) argued the necessity of concentrability in the batch RL. Notably, in the bicausal OT setting, we can draw parallels between Assumption 2 and the χ^2 -divergence $\chi^2(\mathbb{P}||\mathbb{Q}) = \int \frac{d\mathbb{P}^2}{d\mathbb{Q}} - 1$. Assumption 2 is equivalent to considering bicausal transport plans π that exhibit finite χ^2 -divergence with respect to the sampling distribution β . Both the KL-divergence and χ^2 -divergence belong to the f -divergence family. If we set $\beta = \mu \otimes \nu$, the concentrability assumption can be viewed as a regularization utilizing the χ^2 -divergence.

The following result provides an upper bound on the suboptimality of the approximator f in terms of Bellman errors.

Lemma 3 *Given an initial state s_0 , suppose Assumption 2 holds. For any $f \in \mathcal{F}$, we have*

$$2 \left| f_0(s_0) - \int f_1(s_{0:1}) \pi^f(ds_1|s_0) \right| + J_0(s_0; \pi^f) - J_0(s_0; \pi^*) \leq 2\sqrt{CTB(f)},$$

where C is the concentrability coefficient in Assumption 2.

Proof To obtain an upper bound, we note that

$$J_0(s_0; \pi^f) - J_0(s_0; \pi^*) = J_0(s_0; \pi^f) - f_0(s_0) + f_0(s_0) - J_0(s_0; \pi^*). \quad (16)$$

We decompose $f_0(s_0) - J_0(s_0; \pi)$ for a generic bicausal transport π . Using the definition of the objective functional J , we have

$$\begin{aligned} f_0(s_0) - J_0(s_0; \pi) &= f_0(s_0) - \int c(s_{1:T}) \pi(ds_{1:T}|s_0) \\ &= \int [f_0(s_0) - f_1(s_{0:1}) + f_1(s_{0:1}) - \cdots - f_{T-1}(s_{0:T-1}) + f_{T-1}(s_{0:T-1}) \\ &\quad - c(s_{1:T})] \pi(ds_{1:T}|s_0) \\ &= f_0(s_0) - \int f_1(s_{0:1}) \pi(ds_1|s_0) + \int [f_1(s_{0:1}) - \int f_2(s_{0:2}) \pi(ds_2|s_{0:1})] \pi(ds_1|s_0) + \\ &\quad \cdots + \int [f_t(s_{0:t}) - \int f_{t+1}(s_{0:t+1}) \pi(ds_{t+1}|s_{0:t})] \pi(ds_{1:t}|s_0) + \\ &\quad \cdots + \int [f_{T-1}(s_{0:T-1}) - \int c(s_{1:T}) \pi(ds_T|s_{0:T-1})] \pi(ds_{1:T-1}|s_0). \end{aligned}$$

Since π^f is optimal with f , we have

$$\int f_{t+1}(s_{0:t}, s_{t+1}) \pi^f(ds_{t+1}|s_{0:t}) = \mathcal{T}[f_{t+1}](s_{0:t}).$$

Thus,

$$f_0(s_0) - J_0(s_0; \pi^f) = \sum_{t=0}^{T-1} \int \{f_t(s_{0:t}) - \mathcal{T}[f_{t+1}](s_{0:t})\} \pi^f(ds_{1:t}|s_0).$$

Next, we observe that π^* is optimal for the real value function V_t and can be sub-optimal for f_t . Then

$$\int f_{t+1}(s_{0:t}, s_{t+1}) \pi^*(ds_{t+1}|s_{0:t}) \geq \mathcal{T}[f_{t+1}](s_{0:t}).$$

It yields

$$\begin{aligned} f_0(s_0) - J_0(s_0; \pi^*) &= \sum_{t=0}^{T-1} \int \left[f_t(s_{0:t}) - \int f_{t+1}(s_{0:t+1}) \pi^*(ds_{t+1}|s_{0:t}) \right] \pi^*(ds_{1:t}|s_0) \\ &\leq \sum_{t=0}^{T-1} \int \left[f_t(s_{0:t}) - \mathcal{T}[f_{t+1}](s_{0:t}) \right] \pi^*(ds_{1:t}|s_0). \end{aligned}$$

We combine these two inequalities and obtain

$$\begin{aligned} J_0(s_0; \pi^f) - J_0(s_0; \pi^*) &= J_0(s_0; \pi^f) - f_0(s_0) + f_0(s_0) - J_0(s_0; \pi^*) \\ &\leq - \sum_{t=0}^{T-1} \int \{f_t(s_{0:t}) - \mathcal{T}[f_{t+1}](s_{0:t})\} \pi^f(ds_{1:t}|s_0) \\ &\quad + \sum_{t=0}^{T-1} \int \left[f_t(s_{0:t}) - \mathcal{T}[f_{t+1}](s_{0:t}) \right] \pi^*(ds_{1:t}|s_0) \\ &= \sum_{t=1}^{T-1} \int \left[f_t(s_{0:t}) - \mathcal{T}[f_{t+1}](s_{0:t}) \right] \pi^*(ds_{1:t}|s_0) \\ &\quad - \sum_{t=1}^{T-1} \int \{f_t(s_{0:t}) - \mathcal{T}[f_{t+1}](s_{0:t})\} \pi^f(ds_{1:t}|s_0). \end{aligned}$$

By Cauchy-Schwarz inequality and Assumption 2,

$$\begin{aligned} &\left| \sum_{t=1}^{T-1} \int \{f_t(s_{0:t}) - \mathcal{T}[f_{t+1}](s_{0:t})\} \pi^f(ds_{1:t}|s_0) \right| + \left| f_0(s_0) - \int f_1(s_{0:1}) \pi^f(ds_1|s_0) \right| \\ &\leq \sum_{t=0}^{T-1} \left(\int |f_t(s_{0:t}) - \mathcal{T}[f_{t+1}](s_{0:t})|^2 \beta(ds_{1:t}|s_0) \right)^{1/2} \left(\int \left(\frac{\pi^f(ds_{1:t}|s_0)}{\beta(ds_{1:t}|s_0)} \right)^2 \beta(ds_{1:t}|s_0) \right)^{1/2} \\ &\leq \sqrt{C} \sum_{t=0}^{T-1} \left(\int |f_t(s_{0:t}) - \mathcal{T}[f_{t+1}](s_{0:t})|^2 \beta(ds_{1:t}|s_0) \right)^{1/2} \\ &\leq \sqrt{CT} \sqrt{\sum_{t=0}^{T-1} \int |f_t(s_{0:t}) - \mathcal{T}[f_{t+1}](s_{0:t})|^2 \beta(ds_{1:t}|s_0)}, \end{aligned}$$

where we also used the inequality $\sum_{t=0}^{T-1} \sqrt{a_t} \leq \sqrt{T} \sqrt{\sum_{t=0}^{T-1} a_t}$ for $a_t \geq 0$.

The second term with π^* can be bounded similarly. By the definition of Bellman error, we obtain the desired result. \blacksquare

Lemma 3 provides a way to evaluate suboptimality using Bellman errors. In the following two subsections, we further establish bounds on Bellman errors with tools from Rademacher complexity (Mohri et al., 2018) and local Rademacher complexity (Bartlett et al., 2005).

3.2 Bellman Error Bounds by Rademacher Complexity

To quantify the learning capability of a function class, we recall the definition of (empirical) Rademacher complexity from Mohri et al. (2018, Definitions 3.1 and 3.2, Chapter 3):

Definition 4 *Given a function class \mathcal{F} , the empirical Rademacher complexity of \mathcal{F} with respect to a fixed sample (s^1, \dots, s^N) of size N is defined as*

$$\mathbb{E}_\sigma \mathcal{R}_N \mathcal{F} := \mathbb{E}_\sigma \left[\sup_{f \in \mathcal{F}} \frac{1}{N} \sum_{i=1}^N \sigma_i f(s^i) \right], \quad (17)$$

where $\sigma = (\sigma_1, \dots, \sigma_N)$, and σ_i are independent uniform random variables taking values in $\{-1, +1\}$. σ_i is referred to as Rademacher random variables.

The Rademacher complexity of \mathcal{F} is the expectation of the empirical Rademacher complexity over all samples of size N drawn according to β :

$$\mathbb{E} \mathcal{R}_N \mathcal{F} := \mathbb{E}_S [\mathbb{E}_\sigma \mathcal{R}_N \mathcal{F}]. \quad (18)$$

Typically, Rademacher complexity requires the functions to be bounded. Therefore, we impose Assumption 5 as follows:

Assumption 5 *Suppose that all $f_t \in \mathcal{F}_t$, $t = 0, \dots, T$, including the cost function $c(s_{1:T})$, are continuous. Moreover, there exists a constant $K \geq 0$ such that $\|f_t(s_{0:t})\|_\infty \leq K$ for $t = 0, \dots, T$.*

We impose the approximate completeness assumption 6 on function classes \mathcal{F} , which will be verified later in Section 4.2. This assumption states that we can approximate the Bellman operator well at each time step, which is commonly adopted in RL; see Munos and Szepesvári (2008); Chen and Jiang (2019); Duan et al. (2021).

Assumption 6 *Fix an initial state s_0 . For any time $t = 0, \dots, T-1$, there exists $\zeta > 0$ such that*

$$\sup_{f_{t+1} \in \mathcal{F}_{t+1}} \inf_{f_t \in \mathcal{F}_t} \int (f_t(s_{0:t}) - \mathcal{T}[f_{t+1}](s_{0:t}))^2 \beta(ds_{1:t}|s_0) \leq \zeta. \quad (19)$$

Assumption 7 serves to quantify the difference between the true and empirical Bellman operators. If the functions considered are Lipschitz continuous, then Assumption 7 is valid by the duality of the Wasserstein distance W_1 and the fact that $W_1 \leq W_p$, $p \in [1, \infty)$. Another sufficient condition is provided by Eckstein and Nutz (2022, Lemma 3.5).

Assumption 7 *Suppose the initial state s_0 is fixed. Given $t = 0, \dots, T-1$, for any $f_{t+1}(s_{0:t+1}) \in \mathcal{F}_{t+1}$, state $s_{0:t} \in \mathcal{X}_{0:t} \times \mathcal{Y}_{0:t}$, coupling $\pi(ds_{t+1}|s_{0:t}) \in \Pi(\mu^t, \nu^t, s_{0:t})$, and coupling $\hat{\pi}(ds_{t+1}|s_{0:t}) \in \Pi(\hat{\mu}_B^t, \hat{\nu}_B^t, s_{0:t})$, there exists a universal constant $L > 0$, such that*

$$\begin{aligned} & \left| \int f_{t+1}(s_{0:t}, s_{t+1}) \pi(ds_{t+1}|s_{0:t}) - \int f_{t+1}(s_{0:t}, s_{t+1}) \hat{\pi}(ds_{t+1}|s_{0:t}) \right| \\ & \leq L W_p(\pi(ds_{t+1}|s_{0:t}), \hat{\pi}(ds_{t+1}|s_{0:t})). \end{aligned}$$

Next, we consider a function that depends on the convergence of empirical measures for marginals:

$$\Delta(s_{0:t}; B) := [W_p^p(\mu(dx_{t+1}|x_{0:t}), \hat{\mu}_B(dx_{t+1}|x_{0:t})) + W_p^p(\nu(dy_{t+1}|y_{0:t}), \hat{\nu}_B(dy_{t+1}|y_{0:t}))]^{1/p}. \quad (20)$$

With Rademacher complexity, we can derive an upper bound for Bellman errors of the approximator learned through FVI.

Lemma 8 *Assume the initial state s_0 is fixed. Suppose Assumptions 5, 6, and 7 hold. For any $\delta \in (0, 1)$, with probability at least $1 - \delta$ over the draw of an i.i.d. sample $\{s_{0:t}^{n_t}\}$, where $n_t = 1, \dots, N$, $t = 0, \dots, T - 1$, the Bellman error of \hat{f} obtained by FVI satisfies*

$$\begin{aligned} \mathcal{B}(\hat{f}) \leq & T\zeta + \frac{2L^2}{N} \sum_{t=0}^{T-1} \sum_{n_t=1}^N \Delta^2(s_{0:t}^{n_t}; B) + \frac{8LK}{N} \sum_{t=0}^{T-1} \sum_{n_t=1}^N \Delta(s_{0:t}^{n_t}; B) \\ & + 8K \sum_{t=0}^{T-1} \mathbb{E} \mathcal{R}_N \mathcal{F}_t + 4TK^2 \sqrt{\frac{2 \ln(T/\delta)}{N}}. \end{aligned}$$

Proof We first consider the Bellman error at a generic time t . Suppose \hat{f}_{t+1} is obtained. Define an optimizer f_t^* under the distribution $\beta(ds_{1:t}|s_0)$ as

$$f_t^* \in \arg \min_{f_t \in \mathcal{F}_t} \int |f_t(s_{0:t}) - \mathcal{T}[\hat{f}_{t+1}](s_{0:t})|^2 \beta(ds_{1:t}|s_0), \quad (21)$$

where the Bellman operator $\mathcal{T}[\hat{f}_{t+1}]$ relies on the true conditional measures, instead of the empirical measures.

Assumption 5 imposes that functions are bounded by K . Then the loss function satisfies

$$|\mathcal{L}(f_t(s_{0:t}), \mathcal{T}[\hat{f}_{t+1}](s_{0:t})) - \mathcal{L}(f_t^*(s_{0:t}), \mathcal{T}[\hat{f}_{t+1}](s_{0:t}))| \leq 4K^2,$$

for $f_t \in \mathcal{F}_t$.

By Lemma 29 based on Mohri et al. (2018, Theorem 3.3), with probability at least $1 - \delta$ over the draw of an i.i.d. sample $\{s_{0:t}^{n_t}\}$ of size N , the following inequality holds for any $f_t \in \mathcal{F}_t$:

$$\begin{aligned} & \int \mathcal{L}(f_t(s_{0:t}), \mathcal{T}[\hat{f}_{t+1}](s_{0:t})) \beta(ds_{1:t}|s_0) - \int \mathcal{L}(f_t^*(s_{0:t}), \mathcal{T}[\hat{f}_{t+1}](s_{0:t})) \beta(ds_{1:t}|s_0) \\ & \leq \frac{1}{N} \sum_{n_t=1}^N \mathcal{L}(f_t(s_{0:t}^{n_t}), \mathcal{T}[\hat{f}_{t+1}](s_{0:t}^{n_t})) - \frac{1}{N} \sum_{n_t=1}^N \mathcal{L}(f_t^*(s_{0:t}^{n_t}), \mathcal{T}[\hat{f}_{t+1}](s_{0:t}^{n_t})) \\ & \quad + 2\mathbb{E} \mathcal{R}_N \left\{ \mathcal{L}(f_t(s_{0:t}), \mathcal{T}[\hat{f}_{t+1}](s_{0:t})) - \mathcal{L}(f_t^*(s_{0:t}), \mathcal{T}[\hat{f}_{t+1}](s_{0:t})) \middle| f_t \in \mathcal{F}_t \right\} \\ & \quad + 4K^2 \sqrt{\frac{2 \ln(1/\delta)}{N}}. \end{aligned} \quad (22)$$

Next, we bound the right-hand side separately.

By Assumption 7 and Lemma 32, with a given path $s_{0:t}^{n_t}$ and any $f_{t+1} \in \mathcal{F}_{t+1}$, we have the following bound between empirical and true Bellman operators:

$$|\mathcal{T}[f_{t+1}](s_{0:t}^{n_t}) - \widehat{\mathcal{T}}_B[f_{t+1}](s_{0:t}^{n_t})| \leq L\Delta(s_{0:t}^{n_t}; B).$$

In addition, the squared loss satisfies

$$\begin{aligned} \left| \mathcal{L}(f_t, \widehat{\mathcal{T}}_B[\hat{f}_{t+1}]) - \mathcal{L}(f_t, \mathcal{T}[\hat{f}_{t+1}]) \right| &= \left| \widehat{\mathcal{T}}_B^2[\hat{f}_{t+1}] - \mathcal{T}^2[\hat{f}_{t+1}] - 2f_t \widehat{\mathcal{T}}_B[\hat{f}_{t+1}] + 2f_t \mathcal{T}[\hat{f}_{t+1}] \right| \\ &\leq \left| \widehat{\mathcal{T}}_B[\hat{f}_{t+1}] - \mathcal{T}[\hat{f}_{t+1}] \right| \left(\left| \widehat{\mathcal{T}}_B[\hat{f}_{t+1}] \right| + \left| \mathcal{T}[\hat{f}_{t+1}] \right| + 2|f_t| \right). \end{aligned} \quad (23)$$

Under a given path $s_{0:t}^{n_t}$, we can bound the empirical Bellman operator by

$$\begin{aligned} |\widehat{\mathcal{T}}_B[\hat{f}_{t+1}]| &= |\widehat{\mathcal{T}}_B[\hat{f}_{t+1}] - \mathcal{T}[\hat{f}_{t+1}] + \mathcal{T}[\hat{f}_{t+1}]| \leq |\widehat{\mathcal{T}}_B[\hat{f}_{t+1}] - \mathcal{T}[\hat{f}_{t+1}]| + |\mathcal{T}[\hat{f}_{t+1}]| \\ &\leq L\Delta(s_{0:t}^{n_t}; B) + |\mathcal{T}[\hat{f}_{t+1}]|. \end{aligned}$$

Therefore,

$$\left| \mathcal{L}(f_t, \widehat{\mathcal{T}}_B[\hat{f}_{t+1}]) - \mathcal{L}(f_t, \mathcal{T}[\hat{f}_{t+1}]) \right| \leq L\Delta(s_{0:t}^{n_t}; B) \times (4K + L\Delta(s_{0:t}^{n_t}; B)). \quad (24)$$

It implies that

$$\begin{aligned} &\left| \frac{1}{N} \sum_{n_t=1}^N \mathcal{L}(f_t(s_{0:t}^{n_t}), \widehat{\mathcal{T}}_B[\hat{f}_{t+1}](s_{0:t}^{n_t})) - \frac{1}{N} \sum_{n_t=1}^N \mathcal{L}(f_t(s_{0:t}^{n_t}), \mathcal{T}[\hat{f}_{t+1}](s_{0:t}^{n_t})) \right| \\ &\leq \frac{1}{N} \sum_{n_t=1}^N L\Delta(s_{0:t}^{n_t}; B) \times (4K + L\Delta(s_{0:t}^{n_t}; B)). \end{aligned}$$

Hence, the first two terms on the right-hand side of (22) satisfy

$$\begin{aligned} &\frac{1}{N} \sum_{n_t=1}^N \mathcal{L}(f_t(s_{0:t}^{n_t}), \mathcal{T}[\hat{f}_{t+1}](s_{0:t}^{n_t})) - \frac{1}{N} \sum_{n_t=1}^N \mathcal{L}(f_t^*(s_{0:t}^{n_t}), \mathcal{T}[\hat{f}_{t+1}](s_{0:t}^{n_t})) \\ &\leq \frac{1}{N} \sum_{n_t=1}^N \mathcal{L}(f_t(s_{0:t}^{n_t}), \widehat{\mathcal{T}}_B[\hat{f}_{t+1}](s_{0:t}^{n_t})) - \frac{1}{N} \sum_{n_t=1}^N \mathcal{L}(f_t^*(s_{0:t}^{n_t}), \widehat{\mathcal{T}}_B[\hat{f}_{t+1}](s_{0:t}^{n_t})) \\ &\quad + \frac{2}{N} \sum_{n_t=1}^N L\Delta(s_{0:t}^{n_t}; B) \times (4K + L\Delta(s_{0:t}^{n_t}; B)). \end{aligned}$$

To simplify the Rademacher complexity in (22), we first note that

$$\begin{aligned} &\mathbb{E} \mathcal{R}_N \left\{ \left| \mathcal{L}(f_t(s_{0:t}), \mathcal{T}[\hat{f}_{t+1}](s_{0:t})) - \mathcal{L}(f_t^*(s_{0:t}), \mathcal{T}[\hat{f}_{t+1}](s_{0:t})) \right| \middle| f_t \in \mathcal{F}_t \right\} \\ &= \mathbb{E} \mathcal{R}_N \left\{ \left| \mathcal{L}(f_t(s_{0:t}), \mathcal{T}[\hat{f}_{t+1}](s_{0:t})) \right| \middle| f_t \in \mathcal{F}_t \right\}, \end{aligned}$$

thanks to the symmetry of Rademacher random variables. Moreover, we can prove that the squared loss $\mathcal{L}(f_t(s_{0:t}), \mathcal{T}[\hat{f}_{t+1}](s_{0:t}))$ is Lipschitz in the first argument $f_t(s_{0:t})$ with a

Lipschitz constant of $4K$. The proof is similar to (23). Then the contraction property of Rademacher complexity, as described in Shalev-Shwartz and Ben-David (2014, Lemma 26.9) or Lemma 30, yields

$$\mathbb{E}\mathcal{R}_N\left\{\mathcal{L}(f_t(s_{0:t}), \mathcal{T}[\hat{f}_{t+1}](s_{0:t})) \middle| f_t \in \mathcal{F}_t\right\} \leq 4K\mathbb{E}\mathcal{R}_N\{f_t | f_t \in \mathcal{F}_t\} =: 4K\mathbb{E}\mathcal{R}_N\mathcal{F}_t.$$

As a result, the inequality (22) becomes

$$\begin{aligned} & \int \mathcal{L}(f_t(s_{0:t}), \mathcal{T}[\hat{f}_{t+1}](s_{0:t}))\beta(ds_{1:t}|s_0) - \int \mathcal{L}(f_t^*(s_{0:t}), \mathcal{T}[\hat{f}_{t+1}](s_{0:t}))\beta(ds_{1:t}|s_0) \\ & \leq \frac{1}{N} \sum_{n_t=1}^N \mathcal{L}(f_t(s_{0:t}^{n_t}), \hat{\mathcal{T}}_B[\hat{f}_{t+1}](s_{0:t}^{n_t})) - \frac{1}{N} \sum_{n_t=1}^N \mathcal{L}(f_t^*(s_{0:t}^{n_t}), \hat{\mathcal{T}}_B[\hat{f}_{t+1}](s_{0:t}^{n_t})) \\ & \quad + \frac{2}{N} \sum_{n_t=1}^N L\Delta(s_{0:t}^{n_t}; B) \times (4K + L\Delta(s_{0:t}^{n_t}; B)) + 8K\mathbb{E}\mathcal{R}_N\mathcal{F}_t + 4K^2\sqrt{\frac{2\ln(1/\delta)}{N}}. \end{aligned}$$

We take $f_t = \hat{f}_t$. By definition, \hat{f}_t is an optimizer for the empirical loss (8). Then

$$\frac{1}{N} \sum_{n_t=1}^N \mathcal{L}(\hat{f}_t(s_{0:t}^{n_t}), \hat{\mathcal{T}}_B[\hat{f}_{t+1}](s_{0:t}^{n_t})) - \frac{1}{N} \sum_{n_t=1}^N \mathcal{L}(f_t^*(s_{0:t}^{n_t}), \hat{\mathcal{T}}_B[\hat{f}_{t+1}](s_{0:t}^{n_t})) \leq 0.$$

Besides, with Assumption 6, we have

$$\int \mathcal{L}(f_t^*(s_{0:t}), \mathcal{T}[\hat{f}_{t+1}](s_{0:t}))\beta(ds_{1:t}|s_0) \leq \zeta.$$

Hence, the inequality (22) becomes, with probability at least $1 - \delta$,

$$\begin{aligned} & \int \mathcal{L}(\hat{f}_t(s_{0:t}), \mathcal{T}[\hat{f}_{t+1}](s_{0:t}))\beta(ds_{1:t}|s_0) \\ & \leq \zeta + \frac{2}{N} \sum_{n_t=1}^N L\Delta(s_{0:t}^{n_t}; B) \times (4K + L\Delta(s_{0:t}^{n_t}; B)) + 8K\mathbb{E}\mathcal{R}_N\mathcal{F}_t + 4K^2\sqrt{\frac{2\ln(1/\delta)}{N}}. \end{aligned} \tag{25}$$

For the Bellman error $\mathcal{B}(\hat{f})$, we apply the union bound. With probability at least $1 - \delta$,

$$\begin{aligned} \mathcal{B}(\hat{f}) & \leq T\zeta + \frac{2L^2}{N} \sum_{t=0}^{T-1} \sum_{n_t=1}^N \Delta^2(s_{0:t}^{n_t}; B) + \frac{8LK}{N} \sum_{t=0}^{T-1} \sum_{n_t=1}^N \Delta(s_{0:t}^{n_t}; B) \\ & \quad + 8K \sum_{t=0}^{T-1} \mathbb{E}\mathcal{R}_N\mathcal{F}_t + 4TK^2\sqrt{\frac{2\ln(T/\delta)}{N}}. \end{aligned}$$

■

To provide the convergence rate of $\Delta(s_{0:t}^n; B)$, we present two results for the unregularized and entropic OT cases in FVI Algorithm 1, respectively.

For the unregularized case, Fournier and Guillin (2015) provided concentration inequalities for unconditional measures. In our problem, which involves a temporal structure, we assume additional knowledge about the dynamics of marginals in Assumption 9. For instance, in the special case where $P_t = 0$ and $Q_t = 0$, Assumption 9 implies the existence of a universal constant C_0 that is independent of $x_{0:t}$ and $y_{0:t}$, satisfying the exponential moment condition stated in Fournier and Guillin (2015, Theorem 2, Condition (1)). Furthermore, Assumption 9 can encompass more general scenarios, such as autoregressive (AR) models. If the domains are compact, Assumption 9 can be verified under mild conditions.

Assumption 9 (*Light-tailed distribution*) For each time $t = 0, \dots, T-1$, there exist deterministic functions P_t and Q_t , such that

$$\begin{aligned}\mu(dx_{t+1}|x_{0:t}) &\sim P_t(x_{0:t}) + \lambda(dx_{t+1}|x_{0:t}), \\ \nu(dy_{t+1}|y_{0:t}) &\sim Q_t(y_{0:t}) + \eta(dy_{t+1}|y_{0:t}).\end{aligned}$$

For any $x_{0:t} \in \mathcal{X}_{0:t}$ and $y_{0:t} \in \mathcal{Y}_{0:t}$, there exist universal constants $a > p$, $\xi > 0$, $C_0 < \infty$, such that

$$\int_{\mathcal{X}_{t+1}} e^{\xi|x_{t+1}|^a} \lambda(dx_{t+1}|x_{0:t}) \leq C_0, \quad \int_{\mathcal{Y}_{t+1}} e^{\xi|y_{t+1}|^a} \eta(dy_{t+1}|y_{0:t}) \leq C_0.$$

Next, we define a function for the rate of convergence as

$$R(\delta, B) = \begin{cases} \left(\frac{\ln(C_1/\delta)}{C_2 B} \right)^{1/\max\{d/p, 2\}}, & B \geq \frac{\ln(C_1/\delta)}{C_2}, \\ \left(\frac{\ln(C_1/\delta)}{C_2 B} \right)^{p/a}, & B \leq \frac{\ln(C_1/\delta)}{C_2}. \end{cases} \quad (26)$$

Here, constants C_1 and C_2 depend only on p, d, a, ξ , and C_0 . These constants correspond to C and c in Fournier and Guillin (2015, Theorem 2). Our assumption validates Condition (1) in Fournier and Guillin (2015, Theorem 2).

With Assumption 9, we can further characterize $\Delta(s_{0:t}^n; B)$ and provide the convergence rate in terms of $R(\delta, B)$.

Theorem 10 Assume the initial state s_0 is fixed. Suppose Assumptions 5, 6, 7, and 9 hold. With probability at least $1 - \delta$, $\delta \in (0, 1)$, the Bellman error of \hat{f} obtained by FVI satisfies

$$\begin{aligned}\mathcal{B}(\hat{f}) &\leq T\zeta + 2L^2T \cdot 2^{2/p}R\left(\frac{\delta}{(2N+1)T}, B\right)^{2/p} + 8LKT \cdot 2^{1/p}R\left(\frac{\delta}{(2N+1)T}, B\right)^{1/p} \\ &\quad + 8K \sum_{t=0}^{T-1} \mathbb{E} \mathcal{R}_N \mathcal{F}_t + 4TK^2 \sqrt{\frac{2 \ln((2N+1)T/\delta)}{N}}.\end{aligned}$$

Proof By Assumption 9 on the dynamics of μ and ν , we have

$$\begin{aligned}W_p^p(\mu(dx_{t+1}|x_{0:t}^{n_t}), \hat{\mu}_B(dx_{t+1}|x_{0:t}^{n_t})) &= W_p^p(\lambda(dx_{t+1}|x_{0:t}^{n_t}), \hat{\lambda}_B(dx_{t+1}|x_{0:t}^{n_t})), \\ W_p^p(\nu(dy_{t+1}|y_{0:t}^{n_t}), \hat{\nu}_B(dy_{t+1}|y_{0:t}^{n_t})) &= W_p^p(\eta(dy_{t+1}|y_{0:t}^{n_t}), \hat{\eta}_B(dy_{t+1}|y_{0:t}^{n_t})).\end{aligned}$$

Conditioned on $s_{0:t}^{n_t}$, with the uniform moment bound on η and λ in Assumption 9, Fournier and Guillin (2015, Theorem 2) guarantees that with probability at least $1 - \delta_1$,

$$W_p^p(\lambda(dx_{t+1}|x_{0:t}^{n_t}), \hat{\lambda}_B(dx_{t+1}|x_{0:t}^{n_t})) \leq R(\delta_1, B).$$

Similarly, with probability at least $1 - \delta_2$,

$$W_p^p(\eta(dy_{t+1}|y_{0:t}^{n_t}), \hat{\eta}_B(dy_{t+1}|y_{0:t}^{n_t})) \leq R(\delta_2, B).$$

For a generic time t , the inequality (25) holds with probability at least $1 - \delta$. In addition, (25) relies on N samples of $s_{0:t}^{n_t}$. Hence, we apply the union bound by replacing δ with $\delta/(2N + 1)$ and obtain

$$\begin{aligned} & \int \mathcal{L}(\hat{f}_t(s_{0:t}), \mathcal{T}[\hat{f}_{t+1}](s_{0:t})) \beta(ds_{1:t}|s_0) \\ & \leq \zeta + 2L^2 \cdot 2^{2/p} R\left(\frac{\delta}{2N+1}, B\right)^{2/p} + 8LK \cdot 2^{1/p} R\left(\frac{\delta}{2N+1}, B\right)^{1/p} \\ & \quad + 8K\mathbb{E}\mathcal{R}_N\mathcal{F}_t + 4K^2 \sqrt{\frac{2\ln((2N+1)/\delta)}{N}}, \end{aligned}$$

with probability at least $1 - \delta$.

The bound on $\mathcal{B}(\hat{f})$ follows by applying the union bound again and replacing δ with δ/T . \blacksquare

The curse of dimensionality is revealed in Theorem 10 as $R(\delta, B)$ scales with $B^{-1/d}$. It is well-known that entropic regularization can improve sample complexity (Genevay et al., 2019). To quantify the rate of convergence under entropic regularization, we define the function:

$$R(\delta, B; \varepsilon) := \frac{C}{\sqrt{B}} \left(1 + \max\{1, \varepsilon\} e^{C/\varepsilon}\right) \left(\max\{1, \varepsilon^{-d/2}\} + \sqrt{\ln(1/\delta)}\right) + C\varepsilon \ln(C/\varepsilon). \quad (27)$$

Here, C is a sufficiently large constant, which is calculated in the proof of Corollary 11. Importantly, C is independent of the probability δ , sample sizes B and N , and regularization parameter ε . While $R(\delta, B; \varepsilon)$ scales with $1/\sqrt{B}$, it exhibits an exponential dependence on the regularization constant ε , and converges to infinity when $\varepsilon \rightarrow 0$. Furthermore, it is worth noting that Corollary 11 imposes stronger assumptions on the cost function and domains compared to the previous results.

Corollary 11 *Suppose $\mathcal{X}_{0:T}$ and $\mathcal{Y}_{0:T}$ are compact. Assume the initial state s_0 is fixed. The functions $f_t \in \mathcal{F}_t, t = 0, \dots, T$, including the cost function $c(s_{1:T})$, belong to \mathcal{C}^∞ . Moreover, these functions are uniformly bounded by K under Assumption 5. The derivatives of these functions up to a sufficiently high order are uniformly bounded by a universal constant $L' > 0$. Additionally, suppose Assumption 6 holds. Then for a given $\delta \in (0, 1)$, with probability at least $1 - \delta$, the Bellman error of \hat{f} obtained by FVI satisfies*

$$\begin{aligned} \mathcal{B}(\hat{f}) & \leq T\zeta + 2TR \left(\frac{\delta}{(2N+1)T}, B; \varepsilon\right)^2 + 8KTR \left(\frac{\delta}{(2N+1)T}, B; \varepsilon\right) \\ & \quad + 8K \sum_{t=0}^{T-1} \mathbb{E}\mathcal{R}_N\mathcal{F}_t + 4TK^2 \sqrt{\frac{2\ln((2N+1)T/\delta)}{N}}. \end{aligned}$$

The constant C in $R(\delta, B; \varepsilon)$ depends on the constant L' , the uniform bound K , the diameters of \mathcal{X} and \mathcal{Y} , the time horizon T , and the dimension d . Importantly, it is independent of the probability δ , sample sizes B and N , and regularization parameter ε .

Proof We denote C as a constant that may vary line by line.

With compact domains and the Lipschitz property, for any f_{t+1} , Genevay et al. (2019, Theorem 1) proved that

$$0 \leq \mathcal{T}_\varepsilon[f_{t+1}](s_{0:t}^{n_t}) - \mathcal{T}[f_{t+1}](s_{0:t}^{n_t}) \leq C\varepsilon \ln(C/\varepsilon),$$

where C is independent of the states $s_{0:t}^{n_t}$.

The \mathcal{C}^∞ smooth property of f_t and the boundedness of derivatives are used in Genevay et al. (2019, Theorems 2 and 3). Building upon these results, Genevay et al. (2019, Corollary 1) proved that, with probability at least $1 - \delta$,

$$\begin{aligned} & |\mathcal{T}_\varepsilon[f_{t+1}](s_{0:t}^{n_t}) - \widehat{\mathcal{T}}_{\varepsilon, B}[f_{t+1}](s_{0:t}^{n_t})| \\ & \leq 6 \left(1 + e^{C/\varepsilon}\right) \max\{1, \varepsilon^{-d/2}\} \times C/\sqrt{B} + C(1 + \varepsilon e^{C/\varepsilon}) \sqrt{\frac{\ln(1/\delta)}{B}} \\ & \leq \frac{C}{\sqrt{B}} \left(1 + \max\{1, \varepsilon\} e^{C/\varepsilon}\right) \left(\max\{1, \varepsilon^{-d/2}\} + \sqrt{\ln(1/\delta)}\right). \end{aligned}$$

Therefore, with probability at least $1 - \delta$, we have

$$|\mathcal{T}[f_{t+1}](s_{0:t}^{n_t}) - \widehat{\mathcal{T}}_{\varepsilon, B}[f_{t+1}](s_{0:t}^{n_t})| \leq R(\delta, B; \varepsilon).$$

Similar to (24), we can show

$$\left| \mathcal{L}(f_t, \widehat{\mathcal{T}}_{\varepsilon, B}[\hat{f}_{t+1}]) - \mathcal{L}(f_t, \mathcal{T}[\hat{f}_{t+1}]) \right| \leq R(\delta, B; \varepsilon) \times (4K + R(\delta, B; \varepsilon)). \quad (28)$$

The remaining proof is almost the same as in Lemma 8 and Theorem 10. ■

3.3 Bellman Error Bounds by Local Rademacher Complexity

The best rate for Rademacher complexity is typically on the order of $1/\sqrt{N}$. However, this rate may be suboptimal since Rademacher complexity considers global estimates of complexity for all functions in the class. In practice, algorithms may select functions from a smaller subset of the class under consideration. To address this, Bartlett et al. (2005) introduces the concept of local Rademacher complexity (LRC), which provides a faster rate of convergence.

Definition 12 For a generic real-valued function class $\widetilde{\mathcal{F}}$, consider a functional $\mathcal{M} : \widetilde{\mathcal{F}} \rightarrow \mathbb{R}^+$. Given a radius $r > 0$, the LRC is defined as

$$\mathbb{E} \mathcal{R}_N \{f \in \widetilde{\mathcal{F}} | \mathcal{M}(f) \leq r\}.$$

In the LRC, the functional \mathcal{M} is typically chosen as an upper bound on the variance of function f . The selection of the radius r involves a trade-off between the size of the subset in the LRC and the complexity. Bartlett et al. (2005) demonstrated that the optimal choice of r is related to the fixed point of certain functions that possess a sub-root property:

Definition 13 (Bartlett et al. (2005, Definition 3.1)) A function $\psi : [0, \infty) \rightarrow [0, \infty)$ is said to be sub-root if it is nonnegative, nondecreasing, and if $r \mapsto \psi(r)/\sqrt{r}$ is nonincreasing for $r > 0$.

According to Bartlett et al. (2005, Lemma 3.2), a sub-root function that is not the constant function $\psi \equiv 0$ has a unique positive fixed point denoted as r^* , which satisfies the equation $\psi(r^*) = r^*$.

Regarding the LRC as a function of r , Bartlett et al. (2005) considered sub-root functions as upper bounds of the LRC. Bartlett et al. (2005, Theorem 3.3) proved that the fixed point of a properly chosen sub-root function can provide sharper error bounds, as the LRC is smaller than the corresponding global averages.

We adopt the sub-root functions specified in Assumption 14. Note that the $t = 0$ case uses Dirac measures at s_0 .

Assumption 14 Suppose the initial state s_0 is fixed. Consider the FVI output \hat{f} . For each time point $t = 0, \dots, T-1$, define an optimizer f_t^* under the distribution $\beta(ds_{1:t}|s_0)$ as

$$f_t^* \in \arg \min_{f_t \in \mathcal{F}_t} \int |f_t(s_{0:t}) - \mathcal{T}[\hat{f}_{t+1}](s_{0:t})|^2 \beta(ds_{1:t}|s_0).$$

Suppose there exists a sub-root function $\psi_t(r)$ such that

$$\psi_t(r) \geq \mathbb{E} \mathcal{R}_N \left\{ f_t(s_{0:t}) - f_t^*(s_{0:t}) \middle| f_t \in \mathcal{F}_t, \int (f_t(s_{0:t}) - f_t^*(s_{0:t}))^2 \beta(ds_{1:t}|s_0) \leq r \right\}.$$

Denote the unique fixed point of $\psi_t(r)$ as r_t^* .

Later in Proposition 20, we will demonstrate that the fixed point r_t^* has an order of $\ln(N)/N$ for certain neural networks, which is faster than $1/\sqrt{N}$. Consequently, Lemma 15 can enhance the convergence rate with the LRC compared to Lemma 8. However, one drawback is that evaluating LRC is more challenging than Rademacher complexity.

Lemma 15 Suppose the initial state s_0 is fixed and Assumptions 5, 6, 7, and 14 hold. For any $\theta > 1$ and every $\delta \in (0, 1)$, with probability at least $1 - \delta$ over the draw of an i.i.d. sample $\{s_{0:t}^{n_t}\}$, $n_t = 1, \dots, N$, $t = 0, \dots, T-1$, the Bellman error of \hat{f} obtained by FVI satisfies

$$\begin{aligned} \mathcal{B}(\hat{f}) \leq & T\zeta + \frac{\theta}{\theta-1} \left(\frac{2L^2}{N} \sum_{t=0}^{T-1} \sum_{n_t=1}^N \Delta^2(s_{0:t}^{n_t}; B) + \frac{8LK}{N} \sum_{t=0}^{T-1} \sum_{n_t=1}^N \Delta(s_{0:t}^{n_t}; B) \right) \\ & + 22528\theta K^2 \sum_{t=0}^{T-1} r_t^* + \frac{(88 + 832\theta)K^2 T}{N} \ln(T/\delta), \end{aligned}$$

where r_t^* is the fixed point of ψ_t .

Proof The main idea is to apply Bartlett et al. (2005, Theorem 3.3) with a properly chosen function class. At time t when \hat{f}_{t+1} is obtained, we consider the function class as

$$\tilde{\mathcal{F}}_t := \left\{ \mathcal{L}(f_t(s_{0:t}), \mathcal{T}[\hat{f}_{t+1}](s_{0:t})) - \mathcal{L}(f_t^*(s_{0:t}), \mathcal{T}[\hat{f}_{t+1}](s_{0:t})) \middle| f_t \in \mathcal{F}_t \right\}.$$

We verify the assumptions in Bartlett et al. (2005, Theorem 3.3). First, we need to find a functional $\mathcal{M} : \tilde{\mathcal{F}}_t \rightarrow \mathbb{R}^+$ and a constant R_c such that for every $g \in \tilde{\mathcal{F}}_t$, $\text{Var}[g] \leq \mathcal{M}(g) \leq R_c \mathbb{E}[g]$. The expectation and the variance are taken under $\beta(ds_{1:t}|s_0)$. Note that

$$\begin{aligned} & \text{Var} \left[\mathcal{L}(f_t(s_{0:t}), \mathcal{T}[\hat{f}_{t+1}](s_{0:t})) - \mathcal{L}(f_t^*(s_{0:t}), \mathcal{T}[\hat{f}_{t+1}](s_{0:t})) \right] \\ & \leq \mathbb{E} \left[\left(\mathcal{L}(f_t(s_{0:t}), \mathcal{T}[\hat{f}_{t+1}](s_{0:t})) - \mathcal{L}(f_t^*(s_{0:t}), \mathcal{T}[\hat{f}_{t+1}](s_{0:t})) \right)^2 \right] \\ & \leq 16K^2 \mathbb{E} \left[(f_t(s_{0:t}) - f_t^*(s_{0:t}))^2 \right]. \end{aligned}$$

The second inequality follows from the fact that \mathcal{L} is Lipschitz on the first argument with constant $4K$, where Assumption 5 is used. Moreover, the quadratic loss has the following property:

$$\begin{aligned} & \frac{\mathbb{E} \left[\mathcal{L}(f_t(s_{0:t}), \mathcal{T}[\hat{f}_{t+1}](s_{0:t})) \right] + \mathbb{E} \left[\mathcal{L}(f_t^*(s_{0:t}), \mathcal{T}[\hat{f}_{t+1}](s_{0:t})) \right]}{2} \\ & = \mathbb{E} \left[\left(\frac{f_t(s_{0:t}) + f_t^*(s_{0:t})}{2} - \mathcal{T}[\hat{f}_{t+1}](s_{0:t}) \right)^2 \right] + \frac{\mathbb{E} \left[(f_t(s_{0:t}) - f_t^*(s_{0:t}))^2 \right]}{4} \\ & \geq \mathbb{E} \left[\left(f_t^*(s_{0:t}) - \mathcal{T}[\hat{f}_{t+1}](s_{0:t}) \right)^2 \right] + \frac{\mathbb{E} \left[(f_t(s_{0:t}) - f_t^*(s_{0:t}))^2 \right]}{4}. \end{aligned}$$

The second inequality holds because f_t^* is an optimizer. It implies that

$$\begin{aligned} & \mathbb{E} \left[\mathcal{L}(f_t(s_{0:t}), \mathcal{T}[\hat{f}_{t+1}](s_{0:t})) \right] - \mathbb{E} \left[\mathcal{L}(f_t^*(s_{0:t}), \mathcal{T}[\hat{f}_{t+1}](s_{0:t})) \right] \\ & \geq \frac{\mathbb{E} \left[(f_t(s_{0:t}) - f_t^*(s_{0:t}))^2 \right]}{2}. \end{aligned}$$

Therefore,

$$\begin{aligned} & \text{Var} \left[\mathcal{L}(f_t(s_{0:t}), \mathcal{T}[\hat{f}_{t+1}](s_{0:t})) - \mathcal{L}(f_t^*(s_{0:t}), \mathcal{T}[\hat{f}_{t+1}](s_{0:t})) \right] \\ & \leq 32K^2 \mathbb{E} \left[\mathcal{L}(f_t(s_{0:t}), \mathcal{T}[\hat{f}_{t+1}](s_{0:t})) - \mathcal{L}(f_t^*(s_{0:t}), \mathcal{T}[\hat{f}_{t+1}](s_{0:t})) \right]. \end{aligned}$$

Then we can choose the constant $R_c = 32K^2$ and the functional \mathcal{M} as

$$\mathcal{M}(f) := 16K^2 \mathbb{E} \left[(f_t(s_{0:t}) - f_t^*(s_{0:t}))^2 \right].$$

By Bartlett et al. (2005, Theorem 3.3), we assume there exists a sub-root function φ_t with the fixed point r_φ^* . For any $r \geq r_\varphi^*$, φ_t satisfies

$$\varphi_t(r) \geq 32K^2 \mathbb{E} \mathcal{R}_N \left\{ \mathcal{L}(f_t(s_{0:t}), \mathcal{T}[\hat{f}_{t+1}](s_{0:t})) - \mathcal{L}(f_t^*(s_{0:t}), \mathcal{T}[\hat{f}_{t+1}](s_{0:t})) \mid f_t \in \mathcal{F}_t, \mathcal{M}(f_t) \leq r \right\}.$$

We can simplify the right-hand side with the contraction property of Rademacher complexity:

$$\begin{aligned} & \mathbb{E} \mathcal{R}_N \left\{ \mathcal{L}(f_t(s_{0:t}), \mathcal{T}[\hat{f}_{t+1}](s_{0:t})) - \mathcal{L}(f_t^*(s_{0:t}), \mathcal{T}[\hat{f}_{t+1}](s_{0:t})) \middle| f_t \in \mathcal{F}_t, \mathcal{M}(f_t) \leq r \right\} \\ & \leq 4K \mathbb{E} \mathcal{R}_N \left\{ f_t(s_{0:t}) - f_t^*(s_{0:t}) \middle| f_t \in \mathcal{F}_t, \int (f_t(s_{0:t}) - f_t^*(s_{0:t}))^2 \beta(ds_{1:t}|s_0) \leq \frac{r}{16K^2} \right\}. \end{aligned}$$

Hence, we can adopt a simpler sub-root function $\psi_t(r)$ such that

$$\psi_t(r) \geq \mathbb{E} \mathcal{R}_N \left\{ f_t(s_{0:t}) - f_t^*(s_{0:t}) \middle| f_t \in \mathcal{F}_t, \int (f_t(s_{0:t}) - f_t^*(s_{0:t}))^2 \beta(ds_{1:t}|s_0) \leq r \right\}.$$

It is the sub-root function defined in Assumption 14. Moreover, we can set $\varphi_t(r) = 128K^3\psi_t(\frac{r}{16K^2})$. If we denote the fixed point of $\psi_t(r)$ as r_t^* , then $r_\varphi^* \leq 1024K^4r_t^*$ by Lemma 33 from Duan et al. (2021, Lemma G.5) using the definition of sub-root functions.

Now we can apply Bartlett et al. (2005, Theorem 3.3) to the function class $\tilde{\mathcal{F}}_t$ with the sub-root function $\varphi_t(r)$. Denote $c_1 = 704$ and $c_2 = 26$. For any $\theta > 1$ and $\delta \in (0, 1)$, with probability at least $1 - \delta$ over the draw of an i.i.d. sample $\{s_{0:t}^{n_t}\}$ of size N , the following inequality holds for any $f_t \in \mathcal{F}_t$:

$$\begin{aligned} & \int \mathcal{L}(f_t(s_{0:t}), \mathcal{T}[\hat{f}_{t+1}](s_{0:t})) \beta(ds_{1:t}|s_0) - \int \mathcal{L}(f_t^*(s_{0:t}), \mathcal{T}[\hat{f}_{t+1}](s_{0:t})) \beta(ds_{1:t}|s_0) \\ & \leq \frac{\theta}{\theta - 1} \left(\frac{1}{N} \sum_{n_t=1}^N \mathcal{L}(f_t(s_{0:t}^{n_t}), \mathcal{T}[\hat{f}_{t+1}](s_{0:t}^{n_t})) - \frac{1}{N} \sum_{n_t=1}^N \mathcal{L}(f_t^*(s_{0:t}^{n_t}), \mathcal{T}[\hat{f}_{t+1}](s_{0:t}^{n_t})) \right) \quad (29) \\ & \quad + \frac{c_1\theta}{R_c} r_\varphi^* + \frac{11(b-a) + R_c\theta c_2}{N} \ln(1/\delta), \end{aligned}$$

where $[a, b]$ is the range of functions in $\tilde{\mathcal{F}}_t$. We can simplify the right-hand side using the following facts:

- (1) Similar to Lemma 8, we can use the inequality (24) and the fact that \hat{f}_t is an optimizer of the empirical loss to simplify the first two terms on the right-hand side;
- (2) We recall the constants used are given by $c_1 = 704$, $c_2 = 26$, $R_c = 32K^2$, $a = -4K^2$, $b = 4K^2$, $r_\varphi^* \leq 1024K^4r_t^*$.

We obtain

$$\begin{aligned} & \int \mathcal{L}(\hat{f}_t(s_{0:t}), \mathcal{T}[\hat{f}_{t+1}](s_{0:t})) \beta(ds_{1:t}|s_0) \\ & \leq \zeta + \frac{\theta}{\theta - 1} \left(2 \frac{L^2}{N} \sum_{n_t=1}^N \Delta^2(s_{0:t}^{n_t}; B) + 8 \frac{LK}{N} \sum_{n_t=1}^N \Delta(s_{0:t}^{n_t}; B) \right) \quad (30) \\ & \quad + 22528\theta K^2 r_t^* + \frac{(88 + 832\theta)K^2}{N} \ln(1/\delta). \end{aligned}$$

Then the result follows with the union bound. ■

Similar to the Rademacher complexity results in Theorem 10 and Corollary 11, we can further bound $\Delta(s_{0:t}^{n_t}; B)$ with the light-tailed distribution assumption or stronger assumptions as in Corollary 11. We state the corresponding results in Theorem 16 and Corollary 17. The proof is very similar and thus omitted.

Theorem 16 *Suppose the initial state s_0 is fixed and Assumptions 5, 6, 7, 9, and 14 hold. For any $\theta > 1$ and every $\delta \in (0, 1)$, with probability at least $1 - \delta$, the Bellman error of \hat{f} obtained by FVI satisfies*

$$\begin{aligned} \mathcal{B}(\hat{f}) \leq & T\zeta + \frac{\theta}{\theta - 1} \left(2L^2T \cdot 2^{2/p} R \left(\frac{\delta}{(2N+1)T}, B \right)^{2/p} + 8LKT \cdot 2^{1/p} R \left(\frac{\delta}{(2N+1)T}, B \right)^{1/p} \right) \\ & + 22528\theta K^2 \sum_{t=0}^{T-1} r_t^* + \frac{(88 + 832\theta)K^2T}{N} \ln((2N+1)T/\delta), \end{aligned}$$

where r_t^* is the fixed point of ψ_t .

Corollary 17 *Suppose $\mathcal{X}_{0:T}$ and $\mathcal{Y}_{0:T}$ are compact. Assume the initial state s_0 is fixed. The functions $f_t \in \mathcal{F}_t, t = 0, \dots, T$, including the cost function $c(s_{1:T})$, belong to \mathcal{C}^∞ . Moreover, these functions are uniformly bounded by K under Assumption 5. The derivatives of these functions up to a sufficiently high order are uniformly bounded by a universal constant $L' > 0$. Additionally, suppose Assumptions 6 and 14 also hold. Then for a given $\delta \in (0, 1)$, with probability at least $1 - \delta$, the Bellman error of \hat{f} obtained by FVI satisfies*

$$\begin{aligned} \mathcal{B}(\hat{f}) \leq & T\zeta + \frac{\theta}{\theta - 1} \left(2TR \left(\frac{\delta}{(2N+1)T}, B; \varepsilon \right)^2 + 8KTR \left(\frac{\delta}{(2N+1)T}, B; \varepsilon \right) \right) \\ & + 22528\theta K^2 \sum_{t=0}^{T-1} r_t^* + \frac{(88 + 832\theta)K^2T}{N} \ln((2N+1)T/\delta). \end{aligned}$$

The constant C in $R(\delta, B; \varepsilon)$ from (27) depends on the constant L' , the uniform bound K , the diameters of \mathcal{X} and \mathcal{Y} , the time horizon T , and the dimension d . Importantly, it is independent of the probability δ , sample sizes B and N , and regularization parameter ε .

4 Neural Networks as Function Approximators

In this section, we validate the crucial assumptions when neural networks are adopted as approximators. We evaluate the fixed point r_t^* of the sub-root function in Assumption 14 using tools from the covering number. Furthermore, we verify the approximate completeness assumption by recent results of neural networks in Hölder function approximation (Schmidt-Hieber, 2020; Langer, 2021).

Denote the activation function as $\sigma(\cdot)$. For any given depth parameter D and width parameters $\{q_j\}_{j=0}^{D+1}$, a neural network function f can be specified as

$$u \mapsto f(u) = W_D \sigma(W_{D-1} \sigma(W_{D-2} \cdots \sigma(W_1 \sigma(W_0 u + b_1) + b_2) \cdots b_{D-1}) + b_D) + b_{D+1}. \quad (31)$$

Here, W_j is a $q_{j+1} \times q_j$ weight matrix and $b_j \in \mathbb{R}^{q_j}$ is a shift (bias) vector. q_0 is the input dimension. In our setting, the output dimension $q_{D+1} = 1$.

4.1 Calculation of Local Rademacher Complexity with Covering Number

We utilize the covering number to evaluate the LRC.

Definition 18 Consider a metric space (\mathcal{V}, d) and a set $\mathcal{F} \subseteq \mathcal{V}$. For any $\varepsilon > 0$, a set \mathcal{F}^Δ is called a proper ε -cover of \mathcal{F} , if $\mathcal{F}^\Delta \subseteq \mathcal{F}$ and for every $f \in \mathcal{F}$, there is an element $f^\Delta \in \mathcal{F}^\Delta$ satisfying $d(f, f^\Delta) < \varepsilon$. The covering number $\mathcal{N}(\varepsilon, \mathcal{F}, d)$ is the cardinality of a minimal proper ε -cover of \mathcal{F} :

$$\mathcal{N}(\varepsilon, \mathcal{F}, d) := \min\{|\mathcal{F}^\Delta| : \mathcal{F}^\Delta \subseteq \mathcal{F} \text{ is a proper } \varepsilon\text{-cover of } \mathcal{F}\}.$$

When \mathcal{V} is equipped with a norm $\|\cdot\|$, we denote by $\mathcal{N}(\varepsilon, \mathcal{F}, \|\cdot\|)$ the covering number of \mathcal{F} with respect to the metric $d(f, f') := \|f - f'\|$.

Our definition of covering numbers requires the ε -cover to belong to the original set, which is called proper (Anthony and Bartlett, 1999, p. 148). We provide some properties of covering numbers in the Appendix.

In statistical learning theory, we need to consider metrics endowed by samples. Let $\{s^1, \dots, s^N\}$ represent N sample paths, where the time subscripts are omitted for simplicity. We denote β_N as the empirical measure supported on the given sample. For $p \in [1, \infty)$ and a function f , denote $\|f\|_{L_p(\beta_N)} = (\frac{1}{N} \sum_{i=1}^N |f(s^i)|^p)^{1/p}$ as the empirical norm. Set $\|f\|_{L_\infty(\beta_N)} = \max_{1 \leq i \leq n} |f(s^i)|$. $\mathcal{N}(\varepsilon, \mathcal{F}, L_p(\beta_N))$ is the covering number of \mathcal{F} at scale ε with respect to the $L_p(\beta_N)$ norm. Following Mendelson (2003, Definition 3), we define

$$\mathcal{N}_p(\varepsilon, \mathcal{F}) := \sup_N \sup_{\beta_N} \mathcal{N}(\varepsilon, \mathcal{F}, L_p(\beta_N)).$$

Note the difference between $\mathcal{N}_p(\varepsilon, \mathcal{F})$ and $\mathcal{N}(\varepsilon, \mathcal{F}, \|\cdot\|_p)$. $\ln \mathcal{N}_p(\varepsilon, \mathcal{F})$ is sometimes referred to as uniform entropic number (Mendelson, 2003, Definition 3).

Anthony and Bartlett (1999, Theorem 14.5) gave an upper bound on the covering number for neural networks with Lipschitz activation functions. They assumed that ε is less than the uniform norm of the output in each layer times 2. These assumptions hold when using sigmoid activation functions, or ReLU functions with compact domains.

Proposition 19 (Informal) Under the assumptions of Anthony and Bartlett (1999, Theorem 14.5) on a class \mathcal{F} of neural networks with Lipschitz activation functions, for a small $\varepsilon > 0$, the covering number can be bounded by

$$\ln \mathcal{N}_\infty(\varepsilon, \mathcal{F}) \leq C_{NN}(1 + \ln(1/\varepsilon)), \quad (32)$$

where the constant C_{NN} depends on the architecture parameters of the neural networks only.

Proposition 20 Consider any $t = 0, \dots, T-1$. Suppose Assumption 5 holds. If the covering number bound (32) holds for \mathcal{F}_t , then the fixed point $r_t^* \lesssim \frac{\ln(N)}{N}$.

Proof We first fix N sample paths as $s_{0:t}^1, \dots, s_{0:t}^N$ and consider the corresponding empirical measure β_N . Denote $\mathcal{G} := \mathcal{F}_t - \mathcal{F}_t = \{f_1 - f_2 : f_1, f_2 \in \mathcal{F}_t\}$. We omit the time subscript in the following proof since it is clear.

We pick a small $\varepsilon > 0$ satisfying Proposition 19. Then the empirical LRC satisfies

$$\begin{aligned} & \mathbb{E}_\sigma \mathcal{R}_N \{ \tilde{g} : \tilde{g} \in \mathcal{G} - \mathcal{G}, \|\tilde{g}\|_{L_2(\beta_N)} \leq \varepsilon \} \\ & \leq C \sum_{k=1}^{\infty} \frac{\varepsilon}{2^{k-1}} \sqrt{\frac{\ln \mathcal{N}(\varepsilon/2^k, \mathcal{G} - \mathcal{G}, \|\cdot\|_{L_2(\beta_N)})}{N}} \end{aligned} \quad (33)$$

$$\leq C \sum_{k=1}^{\infty} \frac{\varepsilon}{2^{k-1}} \sqrt{\frac{2 \ln \mathcal{N}(\varepsilon/2^{k+1}, \mathcal{G}, \|\cdot\|_{L_2(\beta_N)})}{N}} \quad (34)$$

$$\leq C \sum_{k=1}^{\infty} \frac{\varepsilon}{2^{k-1}} \sqrt{\frac{4 \ln \mathcal{N}(\varepsilon/2^{k+2}, \mathcal{F}_t, \|\cdot\|_{L_2(\beta_N)})}{N}} \quad (35)$$

$$\leq C \sum_{k=1}^{\infty} \frac{\varepsilon}{2^{k-1}} \sqrt{\frac{4 \ln \mathcal{N}_\infty(\varepsilon/2^{k+2}, \mathcal{F}_t)}{N}} \quad (36)$$

$$\leq \frac{C}{\sqrt{N}} \sum_{k=1}^{\infty} \frac{\varepsilon}{2^{k-1}} \sqrt{C_{NN} \left(1 + \ln \left(\frac{2^{k+2}}{\varepsilon} \right) \right)} \quad (37)$$

$$\lesssim \frac{\varepsilon}{\sqrt{N}} (1 + \sqrt{\ln(1/\varepsilon)}), \quad (38)$$

with an absolute constant $C > 0$. The first inequality (33) follows from the proof of Dudley entropy integral, see Wainwright (2019, Theorem 5.22) or Lei et al. (2016, Lemma A.5). The second and the third inequalities (34) – (35) use Lemma 34. The fourth inequality (36) is due to Lemma 35. The fifth inequality (37) is from Proposition 19. The last inequality (38) is due to $\sum_{k=1}^{\infty} \frac{\sqrt{k}}{2^{k-1}} < \infty$ and $\sqrt{a+b} \leq \sqrt{a} + \sqrt{b}$, $a, b \geq 0$. Since the right-hand side does not depend on the sample $s_{0:t}^1, \dots, s_{0:t}^N$, we have

$$\begin{aligned} \mathbb{E} \mathcal{R}_N \{ \tilde{g} : \tilde{g} \in \mathcal{G} - \mathcal{G}, \|\tilde{g}\|_{L_2(\beta_N)} \leq \varepsilon \} &= \mathbb{E} \mathbb{E}_\sigma \mathcal{R}_N \{ \tilde{g} : \tilde{g} \in \mathcal{G} - \mathcal{G}, \|\tilde{g}\|_{L_2(\beta_N)} \leq \varepsilon \} \\ &\lesssim \frac{\varepsilon}{\sqrt{N}} (1 + \sqrt{\ln(1/\varepsilon)}). \end{aligned}$$

By Lei et al. (2016, Theorem 1), we have

$$\begin{aligned} & \mathbb{E} \mathcal{R}_N \left\{ g : g \in \mathcal{G}, \int g^2 d\beta \leq r \right\} \\ & \leq 2 \mathbb{E} \mathcal{R}_N \{ \tilde{g} : \tilde{g} \in \mathcal{G} - \mathcal{G}, \|\tilde{g}\|_{L_2(\beta_N)} \leq \varepsilon \} + \frac{8K_t \ln \mathcal{N}_2(\varepsilon/2, \mathcal{G})}{N} + \sqrt{\frac{2r \ln \mathcal{N}_2(\varepsilon/2, \mathcal{G})}{N}} \\ & \lesssim \frac{\varepsilon}{\sqrt{N}} (1 + \sqrt{\ln(1/\varepsilon)}) + \frac{1 + \ln(1/\varepsilon)}{N} + \sqrt{\frac{r(1 + \ln(1/\varepsilon))}{N}} \\ & \lesssim \frac{\ln N}{N} + \sqrt{\frac{\ln N}{N}} r, \end{aligned}$$

where we set $\varepsilon \propto 1/\sqrt{N}$ in the last inequality. Therefore, we can choose $\psi_t(r) = C(\ln(N)/N + \sqrt{r \ln(N)/N})$ with a large enough constant C independent of r . $\psi_t(r)$ is a sub-root function. Solving $\psi_t(r) = r$ shows that the fixed point satisfies $r_t^* \lesssim \frac{\ln(N)}{N}$.

■

4.2 Approximate Completeness

Thanks to recent advancements in the convergence rates for approximating Hölder functions with neural networks (Schmidt-Hieber, 2020; Langer, 2021), we provide explicit bounds on the approximate completeness in Assumption 6, when the cost function and the approximators are α -Hölder continuous with $\alpha \in (0, 1]$.

4.2.1 HÖLDER SPACE

Definition 21 *Given a Hölder smoothness index $\alpha \in (0, 1]$, denote the domain as $\mathcal{S} \subseteq \mathbb{R}^{d'}$ for some positive integer d' . The Hölder space is given by*

$$\mathcal{H}^\alpha(\mathcal{S}, H) := \left\{ f : \mathcal{S} \rightarrow \mathbb{R} : \|f\|_\infty + \sup_{s, s' \in \mathcal{S}, s \neq s'} \frac{|f(s) - f(s')|}{\|s - s'\|_\infty^\alpha} \leq H \right\}.$$

Assumption 22 is utilized to demonstrate that the Bellman operator on certain appropriate functions is Hölder continuous. Note that Assumption 22 also applies to the cost function, since $f_T = c(s_{1:T})$. Additionally, Assumption 22 is related to conditional kernels along different paths, while Assumption 7 applies to true and empirical measures.

Assumption 22 *Suppose s_0 also varies in a closed subset $\mathcal{S}_0 = \mathcal{X}_0 \times \mathcal{Y}_0$. Given $t = 0, \dots, T-1$, suppose for any $f_{t+1} \in \mathcal{F}_{t+1}$, states $s_{0:t}, s'_{0:t} \in \mathcal{S}_{0:t}$, coupling $\pi(ds_{t+1}|s_{0:t}) \in \Pi(\mu^t, \nu^t, s_{0:t})$, and coupling $\pi(ds_{t+1}|s'_{0:t}) \in \Pi(\mu^t, \nu^t, s'_{0:t})$, there exists a universal constant $L_{t+1} > 0$, such that*

$$\begin{aligned} & \left| \int f_{t+1}(s_{0:t}, s_{t+1}) \pi(ds_{t+1}|s_{0:t}) - \int f_{t+1}(s'_{0:t}, s_{t+1}) \pi(ds_{t+1}|s'_{0:t}) \right| \\ & \leq L_{t+1} W_p(\pi(ds_{t+1}|s_{0:t}), \pi(ds_{t+1}|s'_{0:t})) + L_{t+1} \|s_{0:t} - s'_{0:t}\|_\infty^\alpha. \end{aligned}$$

We introduce the following function, which characterizes the smoothness of conditional kernels of marginals:

$$\Delta(s_{0:t}, s'_{0:t}) := [W_p^p(\mu(dx_{t+1}|x_{0:t}), \mu(dx_{t+1}|x'_{0:t})) + W_p^p(\nu(dy_{t+1}|y_{0:t}), \nu(dy_{t+1}|y'_{0:t}))]^{1/p}. \quad (39)$$

Proposition 23 validates the Hölder smoothness of Bellman operators under Assumption 22 and condition 40.

Proposition 23 *Suppose $\|f_t\|_\infty \leq K_t$ for $t = 1, \dots, T$. Given any $t = 0, \dots, T-1$, suppose Assumption 22 holds with some $L_{t+1} > 0$. Assume there exists a constant H_t such that*

$$\sup_{s_{0:t}, s'_{0:t} \in \mathcal{S}_{0:t}, s_{0:t} \neq s'_{0:t}} \frac{\Delta(s_{0:t}, s'_{0:t})}{\|s_{0:t} - s'_{0:t}\|_\infty^\alpha} \leq (H_t - K_{t+1} - L_{t+1})/L_{t+1}. \quad (40)$$

Then $\mathcal{T}[f_{t+1}] \in \mathcal{H}^\alpha(\mathcal{S}_{0:t}, H_t)$ for $t = 0, \dots, T-1$.

Proof The first step is in the same spirit as Lemma 32. Fix two states $s_{0:t}, s'_{0:t} \in \mathcal{S}_{0:t}$. Denote an optimizer of $\mathcal{T}[f_{t+1}](s_{0:t})$ as $\pi^*(ds_{t+1}|s_{0:t})$. Consider a coupling with disintegration $\mu(dx_{t+1}|x_{0:t}) \otimes \kappa^\mu$ attaining $W_p(\mu(dx_{t+1}|x_{0:t}), \mu(dx_{t+1}|x'_{0:t}))$ and another coupling with disintegration $\nu(dy_{t+1}|y_{0:t}) \otimes \kappa^\nu$ attaining $W_p(\nu(dy_{t+1}|y_{0:t}), \nu(dy_{t+1}|y'_{0:t}))$. Consider $S(\pi^*)$ as the (κ^μ, κ^ν) -shadow of $\pi^*(ds_{t+1}|s_{0:t})$. Then $S(\pi^*) \in \Pi(\mu^t, \nu^t, s'_{0:t})$. We obtain

$$\begin{aligned} & \mathcal{T}[f_{t+1}](s'_{0:t}) - \mathcal{T}[f_{t+1}](s_{0:t}) \\ & \leq \int f_{t+1}(s'_{0:t}, s_{t+1}) S(\pi^*)(ds_{t+1}|s'_{0:t}) - \int f_{t+1}(s_{0:t}, s_{t+1}) \pi^*(ds_{t+1}|s_{0:t}) \\ & \leq L_{t+1} W_p(\pi^*(ds_{t+1}|s_{0:t}), S(\pi^*)(ds_{t+1}|s'_{0:t})) + L_{t+1} \|s_{0:t} - s'_{0:t}\|_\infty^\alpha \\ & \leq L_{t+1} \Delta(s_{0:t}, s'_{0:t}) + L_{t+1} \|s_{0:t} - s'_{0:t}\|_\infty^\alpha. \end{aligned}$$

The second inequality holds due to Assumption 22. The last inequality is from Lemma 31. The other side can be proved similarly. Then

$$|\mathcal{T}[f_{t+1}](s_{0:t}) - \mathcal{T}[f_{t+1}](s'_{0:t})| \leq L_{t+1} \Delta(s_{0:t}, s'_{0:t}) + L_{t+1} \|s_{0:t} - s'_{0:t}\|_\infty^\alpha.$$

The inequality (40) yields

$$\begin{aligned} & \sup_{s_{0:t}, s'_{0:t} \in \mathcal{S}_{0:t}, s_{0:t} \neq s'_{0:t}} \frac{|\mathcal{T}[f_{t+1}](s_{0:t}) - \mathcal{T}[f_{t+1}](s'_{0:t})|}{\|s_{0:t} - s'_{0:t}\|_\infty^\alpha} \\ & \leq L_{t+1} \times (H_t - K_{t+1} - L_{t+1})/L_{t+1} + L_{t+1} \\ & = H_t - K_{t+1}. \end{aligned}$$

As $\|\mathcal{T}[f_{t+1}](s_{0:t})\|_\infty \leq K_{t+1}$ with the boundedness assumption, it follows that $\mathcal{T}[f_{t+1}] \in \mathcal{H}^\alpha(\mathcal{S}_{0:t}, H_t)$ by the Definition 21. \blacksquare

In the following two subsections, we explore specific function classes that satisfy Assumptions 22 and 6, including sparse ReLU networks and sigmoid networks. By appropriately choosing the neural network architecture, we can obtain explicit bounds on approximate completeness (Schmidt-Hieber, 2020; Langer, 2021).

4.2.2 SPARSE RELU NETWORK

Denote the ReLU activation function as $\sigma(u) := \max\{u, 0\}$. We restrict to the class of ReLU networks where most parameters are zero.

Definition 24 *With a given depth D , width $\{q_j\}_{j=0}^{D+1}$, sparsity γ , and uniform bound K , the sparse ReLU network is defined as*

$$\begin{aligned} \mathcal{F}(D, \{q_j\}_{j=0}^{D+1}, \gamma, K) &:= \{f : f \text{ specified as in (31)}, \quad \sigma(u) = \max\{u, 0\}, \quad b_{D+1} = 0, \\ & \max_{j=0, \dots, D} \|W_j\|_\infty \vee \|b_j\|_\infty \leq 1, \quad \sum_{j=0}^D \|W_j\|_0 + \|b_j\|_0 \leq \gamma, \\ & \|f\|_\infty \leq K\}, \end{aligned}$$

with the convention that $b_0 = 0$.

A more explicit upper bound on the covering number is also available for sparse ReLU networks. The proof is a slight extension of Suzuki (2019, Lemma 3) and is thus omitted. Additionally, Schmidt-Hieber (2020, Lemma 5) also provided a similar estimate.

Proposition 25 (Suzuki (2019, Lemma 3)) *The covering number of sparse ReLU networks $\mathcal{F}_t := \mathcal{F}(D_t, \{q_j^t\}_{j=0}^{D_t+1}, \gamma_t, K_t)$ can be bounded by*

$$\ln \mathcal{N}_\infty(\delta, \mathcal{F}_t) \leq \gamma_t \ln \left((D_t + 1)/\delta \prod_{j=0}^{D_t} (q_j^t + 1)^2 \right) \leq C_{ReLU}(1 + \ln(1/\delta)),$$

where the constant C_{ReLU} is independent of δ and only depends on the depth D_t , width $\{q_j^t\}_{j=0}^{D_t+1}$, and sparsity γ_t .

Thanks to Schmidt-Hieber (2020, Theorem 5), we have the following result on approximate completeness, under the assumption that the domains are compact.

Proposition 26 *Suppose*

- (1) $\mathcal{X}_t = \mathcal{Y}_t = [0, 1]^d$ for $t = 0, 1, \dots, T$;
- (2) the cost $\|c(s_{1:T})\|_\infty \leq K_T$ and satisfies Assumption 22 with some $L_T > 0$ and $\alpha \in (0, 1]$;
- (3) for $t = 0, \dots, T-1$, the function class $\mathcal{F}_t = \mathcal{F}(D_t, \{q_j^t\}_{j=0}^{D_t+1}, \gamma_t, K_t)$ with some D_t , $\{q_j^t\}_{j=0}^{D_t+1}$, γ_t , and K_t specified below;
- (4) inequality (40) holds for large enough $H_t > 0$ at each $t = 0, \dots, T-1$.

Then

- (a) $\mathcal{T}[f_{t+1}] \in \mathcal{H}^\alpha(\mathcal{S}_{0:t}, H_t)$ for $t = 0, \dots, T-1$;
- (b) ReLU network parameters are specified backwardly as follows: Suppose \mathcal{F}_{t+1} is chosen. Denote $d_t := (t+1)d$ for simplicity. For \mathcal{F}_t , consider any integers $m_t \geq 1$ and $G_t \geq \max\{(\alpha+1)^{d_t}, (H_t+1)e^{d_t}\}$, set width $\{q_j^t\}_{j=0}^{D_t+1} = \{d_t, 6(d_t+1)G_t, \dots, 6(d_t+1)G_t, 1\}$, depth $D_t = 8 + (m_t+5)(1 + \lceil \log_2(d_t) \rceil)$, sparsity $\gamma_t \leq 141(d_t + \alpha + 1)^{3+d_t}G_t(m_t+6)$, and uniform bound $K_t = (2H_t+1)(1 + d_t^2 + \alpha^2)6^{d_t}G_t2^{-m_t} + H_t3^\alpha G_t^{-\frac{\alpha}{d_t}} + K_{t+1}$;
- (c) at time $t = 0, \dots, T-1$, the approximate completeness assumption 6 holds with $\zeta_t = (K_t - K_{t+1})^2$.

Proof We prove the claims by backward induction.

At time $T-1$, since \mathcal{F}_T only contains the cost function $c(s_{1:T})$ and conditions (2) and (4) hold, then Proposition 23 shows that $\mathcal{T}[f_T] \in \mathcal{H}^\alpha(\mathcal{S}_{0:T-1}, H_{T-1})$ with a sufficiently large $H_{T-1} > K_T + L_T$. Hence, we can apply Schmidt-Hieber (2020, Theorem 5): There exists a sparse ReLU network $\tilde{f} \in \mathcal{F}(D_{T-1}, \{q_j^{T-1}\}_{j=0}^{D_{T-1}+1}, \gamma_{T-1}, \infty)$ with parameters defined in (b), such that

$$\begin{aligned} \|\tilde{f} - \mathcal{T}[f_T]\|_\infty &\leq (2H_{T-1} + 1)(1 + d_{T-1}^2 + \alpha^2)6^{d_{T-1}}G_{T-1}2^{-m_{T-1}} + H_{T-1}3^\alpha G_{T-1}^{-\frac{\alpha}{d_{T-1}}} \\ &:= K_{T-1} - K_T. \end{aligned}$$

Since $\|\mathcal{T}[f_T]\|_\infty \leq K_T$, then we can restrict the function class \mathcal{F}_{T-1} to be bounded by K_{T-1} . Therefore,

$$\begin{aligned} & \sup_{f_T \in \mathcal{F}_T} \inf_{f_{T-1} \in \mathcal{F}_{T-1}} \int (f_{T-1}(s_{0:T-1}) - \mathcal{T}[f_T](s_{0:T-1}))^2 \beta(ds_{1:T-1}|s_0) \\ & \leq \sup_{f_T \in \mathcal{F}_T} \inf_{f_{T-1} \in \mathcal{F}_{T-1}} \|f_{T-1}(s_{0:T-1}) - \mathcal{T}[f_T](s_{0:T-1})\|_\infty^2 \\ & \leq (K_{T-1} - K_T)^2 := \zeta_{T-1}. \end{aligned}$$

Then claim (c) holds with ζ_{T-1} .

At time $T - 2$, we first observe that a ReLU network is a composition of Lipschitz functions and thus is also Lipschitz. Furthermore, under condition (1), the domain is compact. Then Assumption 22 holds for functions in \mathcal{F}_{T-1} with a sufficiently large L_{T-1} , since the inputs and parameters of sparse ReLU networks are uniformly bounded. In Condition (4), we can choose $H_{T-2} > L_{T-1} + K_{T-1}$. It is important to note that L_{T-1} and K_{T-1} are determined by the parameters from the previous step T . Proposition 23 shows that $\mathcal{T}[f_{T-1}] \in \mathcal{H}^\alpha(\mathcal{S}_{0:T-2}, H_{T-2})$ for $f_{T-1} \in \mathcal{F}_{T-1}$. The remaining proof repeats the previous arguments. Hence, we obtain the results for $t = T - 2, \dots, 0$ in a backward manner. \blacksquare

4.2.3 SIGMOID NEURAL NETWORKS

Since Corollaries 11 and 17 regarding the sample complexity with entropic regularization require a smooth function class, we provide the corresponding result for neural networks with the sigmoid activation function, defined as follows:

$$\sigma(u) = \frac{1}{1 + e^{-u}}.$$

Definition 27 *With a given depth D , width q , and parameter uniform bound U , the sigmoid neural network is defined as*

$$\begin{aligned} \Sigma(D, q, U, K) := \{f : f \text{ specified as in (31), } \sigma(u) = \frac{1}{1 + e^{-u}}, \quad q_D = \dots = q_1 = q, \\ \max_{j=0, \dots, D} \|W_j\|_\infty \vee \|b_{j+1}\|_\infty \leq U, \quad \|f\|_\infty \leq K\}. \end{aligned}$$

Definition 27 adheres to the specification in Langer (2021) and does not impose any sparsity constraint. By utilizing Langer (2021, Theorem 1), we establish the approximate completeness result for sigmoid neural networks.

Proposition 28 *Suppose*

- (1) $\mathcal{X}_t = \mathcal{Y}_t = [-a, a]^d$ with some $a \in [1, \infty)$, for all $t = 0, 1, \dots, T$;
- (2) the cost $\|c(s_{1:T})\|_\infty \leq K_T$ and satisfies Assumption 22 with some $L_T > 0$ and $\alpha \in (0, 1]$;
- (3) for $t = 0, \dots, T - 1$, the function class $\mathcal{F}_t = \Sigma(D_t, q_t, U_t, K_t)$ with some D_t, q_t, U_t , and K_t specified below;

(4) inequality (40) holds for large enough $H_t > 0$ at each $t = 0, \dots, T - 1$.

Then

(a) $\mathcal{T}[f_{t+1}] \in \mathcal{H}^\alpha(\mathcal{S}_{0:t}, H_t)$ for $t = 0, \dots, T - 1$;

(b) sigmoid network parameters are specified backwardly as follows: Suppose \mathcal{F}_{t+1} is chosen. Denote constant $d_t := (t + 1)d$ for simplicity. For \mathcal{F}_t , consider any integers M_t satisfying $M_t^{2\alpha} \geq \max\{2c_{2,t}(\max\{a, K_{t+1}\})^3, c_{3,t}, 2^{d_t}, 12d_t\}$, for some constant $c_{2,t}$ and $c_{3,t}$. Set depth $D_t = 8 + \lceil \log_2(d_t) \rceil$, width $q_t = 2^{d_t}(2M_t^{d_t}(1 + d_t)^2 + 2M_t^{d_t}(1 + d_t) + 13d_t)$, and uniform parameter bound $U_t = c_{4,t}(\max\{a, K_{t+1}\})^{11}e^{6 \times 2^{2(d_t+1)+1}ad_t}M_t^{16\alpha+2d_t+9}$. Moreover, let $K_t := K_{t+1} + \frac{c_{5,t}(\max\{a, K_{t+1}\})^3}{M_t^{2\alpha}}$ for some constant $c_{5,t} > 0$;

(c) at time $t = 0, \dots, T - 1$, the approximate completeness assumption 6 holds with $\zeta_t := (K_t - K_{t+1})^2$.

Proof We prove the results backwardly in time t .

At time $T - 1$, we first note that \mathcal{F}_T only contains the cost function $c(s_{1:T})$. Under conditions (2) and (4), we have $\mathcal{T}[f_T] \in \mathcal{H}^\alpha(\mathcal{S}_{0:T-1}, H_{T-1})$ by Proposition 23, where the constant $H_{T-1} > L_T + K_T$. By Lemma 36, we can extend $\mathcal{T}[f_T]$ to the whole domain \mathbb{R}^{Td} as follows:

$$g(s_{0:T-1}) := \inf\{\mathcal{T}[f_T](u_{0:T-1}) + (H_{T-1} - K_T)\|s_{0:T-1} - u_{0:T-1}\|_\infty^\alpha, \quad u_{0:T-1} \in \mathcal{S}_{0:T-1}\}.$$

Since $\mathcal{T}[f_T]$ is α -Hölder continuous with constant $H_{T-1} - K_T$ on $\mathcal{S}_{0:T-1}$, we can verify that g is α -Hölder continuous with the same constant $H_{T-1} - K_T$ on \mathbb{R}^{Td} . Moreover, $g = \mathcal{T}[f_T]$ on $\mathcal{S}_{0:T-1}$.

Then we can apply Langer (2021, Theorem 1): There exists a neural network $f_{T-1} \in \Sigma(D_{T-1}, q_{T-1}, U_{T-1}, \infty)$, with constants defined in (b), such that

$$\|f_{T-1} - \mathcal{T}[f_T]\|_{\infty, \mathcal{S}_{0:T-1}} \leq \frac{c_{5,T-1}(\max\{a, K_T\})^3}{M_{T-1}^{2\alpha}},$$

where the uniform norm is over $\mathcal{S}_{0:T-1}$. Then we can choose the uniform upper bound $K_{T-1} = K_T + \frac{c_{5,T-1}(\max\{a, K_T\})^3}{M_{T-1}^{2\alpha}}$. The approximate completeness assumption at time $T - 1$ is valid with $(K_{T-1} - K_T)^2$.

For a generic time t , note that the sigmoid activation function is Lipschitz. Parameters and inputs of sigmoid networks in \mathcal{F}_{t+1} are uniformly bounded. Then all functions in \mathcal{F}_{t+1} are Lipschitz with a universal constant L_{t+1} . The constant $H_t > L_{t+1} + K_{t+1}$ is chosen backwardly. Therefore, the remaining proof becomes similar to the arguments above. ■

5 Numerical Results

5.1 Gaussian Data

It is rare for OT problems to have explicit solutions, even in the single-period case. One exception is the Gaussian distribution. Hence, for the numerical test, we consider μ and ν

as Gaussian distributions with linear dynamics:

$$\begin{aligned} x_{t+1} &= x_t + \lambda_t, & \lambda_t &\sim N(0, \Sigma_x), \\ y_{t+1} &= y_t + \eta_t, & \eta_t &\sim N(0, \Sigma_y). \end{aligned}$$

Here, $x_t \in \mathbb{R}^d$ and $y_t \in \mathbb{R}^d$ are two AR(1) processes in the context of time-series analysis. The white Gaussian noise processes λ_t and η_t are independent, with mean zero and constant covariance matrices Σ_x and Σ_y , respectively. The bicausal OT problem with quadratic cost is defined as follows:

$$\inf_{\pi \in \Pi_{bc}(\mu, \nu, x_0, y_0)} \int \sum_{t=1}^T (x_t - y_t)^2 \pi(dx_{1:T}, dy_{1:T} | x_0, y_0).$$

The explicit solution to this problem is given by

$$T|x_0 - y_0|^2 + \frac{T(T+1)}{2} \left(\text{tr}[\Sigma_x] + \text{tr}[\Sigma_y] - 2\text{tr} \left[\sqrt{\sqrt{\Sigma_x} \Sigma_y \sqrt{\Sigma_x}} \right] \right).$$

This result can be proven similarly to Han (2023, Corollary 2.2) by applying the single-period case (Givens and Shortt, 1984) repeatedly. Additionally, it is worth noting that the single-period case is closely related to the Bures metric.

In the experiment, we consider an agent that lacks knowledge of the actual underlying distribution but can sample data from it. From a theoretical standpoint, Gaussian data do not have compact support, which violates the assumptions in Propositions 26 and 28. However, the FVI algorithm is still applicable, and the empirical distribution has bounded support. To assess the effectiveness of our method, we compare it with the LP and adapted Sinkhorn algorithms (Eckstein and Pammer, 2023). All experiments were performed on a laptop equipped with an Intel Core i5-12500H 3.10GHz CPU and an NVIDIA RTX 3050 Ti Laptop GPU. The PyTorch library was utilized for neural network implementation.

5.2 One-dimensional Data

We begin by examining the one-dimensional case ($d = 1$). The variances are fixed as $\Sigma_x = 1.0$ and $\Sigma_y = 0.5^2$. The initial values are set as $x_0 = 1.0$ and $y_0 = 2.0$.

5.2.1 LINEAR PROGRAMMING METHOD

Both the LP and adapted Sinkhorn methods require a discrete distribution to approximate the continuous distribution μ and ν . To accomplish this, we employ a non-recombining binomial tree construction as follows. Initially, at time $t = 1$, we simulate x_1 and partition the samples into two sets. We then use the mean and frequency of each set to create two nodes in the tree. Next, we sample x_2 conditioned on each x_1 . At time 2, there will be four nodes in total, as the middle two nodes are almost surely not recombined. We repeat this procedure until time T . Both the LP and adapted Sinkhorn algorithms consider this tree as the underlying discrete distribution. Figure 1 illustrates an example of a non-recombining binomial tree. Since the agent does not possess knowledge of the true distribution, constructing a recombining binomial tree to reduce the number of nodes

becomes challenging. Additionally, we also explored the adapted empirical measures with k -means as proposed in Backhoff-Veraguas et al. (2022); Eckstein and Pammer (2023). However, since the number of cubes after the partition is on the order of $N^{1/(T+1)}$ (Backhoff-Veraguas et al., 2022, Definition 1.2), it requires a large sample size N even for two cubes under long time horizons. Hence, we consider the non-recombining tree since it is more applicable.

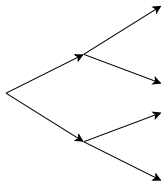


Figure 1: A non-recombining binomial tree.

Horizon T	Actual	Estimated mean (SD)	Average runtime
1	1.25	1.217 (0.102)	0.102
2	2.75	2.734 (0.243)	0.270
3	4.5	4.262 (0.488)	0.587
4	6.5	6.295 (0.401)	1.311
5	8.75	8.416 (0.600)	2.909
6	11.25	10.414 (1.028)	6.201
7	14.0	12.713 (1.071)	13.733
8	17.0	16.114 (0.902)	32.178
9	20.25	19.051 (1.417)	83.298
10	23.75	22.649 (1.277)	248.249
11	27.5	25.557 (1.646)	794.041

Table 1: The LP method with backward induction for bicausal OT.

For the LP and adapted Sinkhorn algorithms, we utilize the implementation by Eckstein and Pammer (2023), which can be found at <https://github.com/stephaneckstein/aotnumerics>. The LP formulation can be implemented using backward induction or directly as described in Eckstein and Pammer (2023, Lemma 3.11). We first test the LP formulation in Eckstein and Pammer (2023, Lemma 3.11), employing the Gurobi solver with an academic license. In the case of $T = 10$, we observed that this method took longer than 1000 seconds to finish. Gurobi reported the model had 701098 rows, 1048576 columns, and 23068672 nonzeros, even after the presolve phase (Andersen and Andersen, 1995; Achterberg et al., 2020) to reduce the problem size. Consequently, we resorted to using the LP with backward induction, which solves an OT problem of shape 2×2 at each time and state. The estimated results are presented in Table 1. For each configuration, we conducted 10 instances to compute the mean and standard deviation (SD). The average runtime, measured in seconds per instance, includes the data sampling time as well. Table 1 demonstrates that the non-recombining tree can effectively approximate the AR(1) model, yielding accurate means and low variances. However, the runtime grows rapidly, indicating

that the LP method does not scale well. We also conducted tests for the case of $T = 12$ and found that the runtime was approximately 2600 seconds.

5.2.2 ADAPTED SINKHORN METHOD

Table 2 demonstrates the remarkable accuracy of the adapted Sinkhorn method. The stopping criterion is when the change in dual values is less than 10^{-4} . The actual values presented in Tables 1 and 2 correspond to continuous distributions. Therefore, the errors between the actual and estimated values also include the approximation errors resulting from discretization with binomial trees.

We observe that the runtime of the adapted Sinkhorn method increases rapidly as the time horizon expands. Interestingly, the adapted Sinkhorn method is even slower than the LP method. This can be attributed to the fact that, in order to obtain the potential functions, the adapted Sinkhorn method (Eckstein and Pammer, 2023, Lemma 6.6) needs to iterate over all possible scenarios of (x_t, y_t) for each time t . In a non-recombining binomial tree model, the number of these scenarios grows exponentially with the horizon T . Our experimental results do not contradict the findings of Eckstein and Pammer (2023). When the time horizon is short (as in $T = 2$ in Eckstein and Pammer (2023)), this drawback of the adapted Sinkhorn algorithm is mitigated, and it can be faster if the number of possible scenarios is moderate, but not excessively small.

Moreover, although the entropic OT converges to the unregularized OT when $\varepsilon \rightarrow 0$, the Sinkhorn algorithm can encounter numerical instability issues when ε is small. As the time horizon T increases, a larger value of ε becomes necessary. This introduces a trade-off between stability, accuracy, and speed by varying ε . Compared with the FVI results in Table 3, we observe that for similar levels of accuracy, the adapted Sinkhorn method is much slower for longer time horizons. Additionally, when $T \geq 20$, both the LP and adapted Sinkhorn methods fail to converge within a reasonable time.

Horizon T	Actual	Estimated mean (SD)	Average runtime	ε in entropic regularization
1	1.25	1.201 (0.103)	0.087	0.1
2	2.75	2.701 (0.251)	0.313	0.1
3	4.5	4.215 (0.488)	0.815	0.1
4	6.5	6.229 (0.389)	2.320	0.1
5	8.75	8.297 (0.656)	8.067	0.1
6	11.25	10.332 (1.014)	22.600	0.2
7	14.0	12.662 (1.079)	39.994	0.4
8	17.0	16.085 (0.915)	205.034	0.6
9	20.25	19.132 (1.416)	517.958	0.8
10	23.75	22.874 (1.297)	1443.557	1.0

Table 2: The adapted Sinkhorn method for bicausal OT.

5.2.3 THE FVI ALGORITHM

In the FVI algorithm, we define the sampling distribution as $\beta = \mu \otimes \nu$. Suppose the agent knows that the true value function is separable in time and state variables. We use a neural

network class \mathcal{F}_t with the same architecture across different time steps. The architecture is specified as $F_1(T-t)F_2(x_t, y_t) + F_3(T-t)$, where F_1, F_2 and F_3 are learnable approximators. In particular, F_1 and F_3 are quadratic functions of $T-t$, while F_2 is a multilayer ReLU neural network with a depth $D = 2$ and hidden width $q_j = 8$. We have not enforced sparsity in the implementation. Since F_1, F_2 , and F_3 are not identifiable, we introduce a sigmoid function to scale the last output of F_2 into the range $(0, 1)$. The network is initialized using the default method in PyTorch. Our code is available at <https://github.com/hanbingyan/FVIOT>.

For optimization, we utilize the Adam optimizer with a learning rate of 0.01. Gradients and parameters are truncated elementwise to the range of $[-1, 1]$ in each gradient descent step. Through experiments, we observe that the smooth L_1 loss in PyTorch outperforms the squared loss function, possibly because it is less affected by outliers. The smooth L_1 loss function, closely related to the Huber loss, is defined as follows:

$$l(f, v) = \begin{cases} \frac{1}{2\tau}(f - v)^2, & \text{if } |f - v| < \tau, \\ |f - v| - \tau/2, & \text{otherwise.} \end{cases}$$

The default threshold value is $\tau = 1.0$.

Table 3 presents the estimation results for the FVI algorithm with the unregularized empirical OT. To prevent overfitting, we reduce the number of gradient steps (G) as the time horizon increases. Other hyperparameters are fixed, including a batch size of 128 for gradient descent, 2000 sample paths (N), and a sample size of 50 for the empirical OT (B). Although the estimation error is higher compared to the LP and adapted Sinkhorn methods, it remains within moderate and acceptable levels. As expected, the variance increases with the horizon. The reported runtime includes data sampling. For small horizons, our method requires more time. However, the computational burden increases linearly. The FVI algorithm becomes faster than the LP and adapted Sinkhorn methods for longer horizons. Based on these observations, we assert that the FVI method provides acceptable accuracy and exhibits scalability.

Horizon T	Actual	Estimated mean (SD)	Average runtime	Gradient steps G
1	1.25	1.311 (0.049)	10.592	50
2	2.75	2.932 (0.181)	15.655	50
3	4.5	5.031 (0.306)	22.184	50
4	6.5	7.261 (0.534)	28.713	50
5	8.75	9.710 (0.951)	35.560	50
6	11.25	12.315 (1.171)	41.256	40
7	14.0	14.901 (1.354)	47.410	30
8	17.0	17.907 (2.660)	55.071	20
9	20.25	21.392 (2.426)	60.681	20
10	23.75	24.455 (3.610)	66.435	20
20	72.5	72.020 (8.172)	131.445	20
40	245.0	235.266 (38.341)	257.693	20

Table 3: FVI with one-dimensional data.

5.3 Multidimensional Data

The implementations of the LP and adapted Sinkhorn algorithms in Eckstein and Pammer (2023) do not account for multidimensional data. However, our FVI method offers a uniform framework for handling such data. To illustrate, we assume that the covariance matrices are diagonal. Consider $x_0 = \mathbf{1}_d$, $y_0 = 2\mathbf{1}_d$, $\Sigma_x = 1.1^2 I_d$, and $\Sigma_y = 0.1^2 I_d$. We set the time horizon $T = 5$.

The empirical OT suffers from the curse of spatial dimensionality, necessitating larger sample sizes (B) and a greater number of paths (N). In our experiment, we set these hyperparameters to $N = 4000$, $B = 300$, and $G = 400$. Since the actual values are large, we do not impose any parameter constraints in this particular experiment. The results are summarized in Table 4. We observe accurate estimation outcomes for low-dimensional cases with $d = 5$ and $d = 10$. As anticipated, estimates become less accurate as the dimension d increases. It is worth noting that the runtime of our method solely relies on the hyperparameters and remains unaffected by the input dimension d .

Horizon T	Dimension d	Actual	Estimate mean (SD)	Average runtime
$T = 5$	$d = 5$	100.0	99.861 (3.421)	336.310
$T = 5$	$d = 10$	200.0	191.948 (6.900)	358.793
$T = 5$	$d = 15$	300.0	268.245 (13.931)	336.887
$T = 5$	$d = 20$	400.0	351.073 (7.751)	334.874

Table 4: FVI with multidimensional data.

6 Concluding Remarks

In summary, our FVI algorithm is well-suited for tackling problems with long time horizons and extensive state spaces. However, if the horizon is short and the state space is small, the LP and Sinkhorn algorithms are more appropriate.

One drawback of the FVI algorithm is its tendency to exhibit larger variance and sensitivity to data with high volatility. While the discretization error may be more pronounced when dealing with a volatile true distribution, the estimated values produced by the FVI algorithm deteriorate more severely compared to the Sinkhorn algorithm. This disparity could potentially be attributed to the ERM framework employed by the FVI. A future direction is to mitigate the variance in the FVI estimations.

Acknowledgments and Disclosure of Funding

Erhan Bayraktar is partially supported by the National Science Foundation under grant DMS-2106556 and by the Susan M. Smith chair.

Appendix A. Rademacher Complexity

Lemma 29 (A slight extension to Mohri et al. (2018, Theorem 3.3)) Let \mathcal{G} be a family of functions mapping from \mathcal{Z} to $[-a, a]$ for some $a > 0$. Then, for any $\delta \in (0, 1)$, with probability at least $1 - \delta$ over the draw of an i.i.d. sample $\{z_i\}$ of size N , the following holds for all $g \in \mathcal{G}$:

$$\mathbb{E}[g(z)] \leq \frac{1}{N} \sum_{i=1}^N g(z_i) + 2\mathbb{E}\mathcal{R}_N \mathcal{G} + a\sqrt{\frac{2\ln(1/\delta)}{N}}. \quad (41)$$

Lemma 30 (Shalev-Shwartz and Ben-David, 2014, Lemma 26.9, contraction property) Let $A \subseteq \mathbb{R}^N$ be a set of vectors. Similar to the empirical Rademacher complexity (17), define

$$\mathbb{E}_\sigma \mathcal{R}_N A := \mathbb{E}_\sigma \left[\sup_{a \in A} \frac{1}{N} \sum_{i=1}^N \sigma_i a_i \right].$$

For each $i = 1, \dots, N$, let $\phi_i : \mathbb{R} \rightarrow \mathbb{R}$ be an L -Lipschitz function, namely $|\phi_i(x) - \phi_i(y)| \leq L|x - y|$, $\forall x, y \in \mathbb{R}$. For $a \in \mathbb{R}^N$, let $\phi(a)$ denote the vector $(\phi_1(a_1), \dots, \phi_N(a_N))$. Let $\phi \circ A := \{\phi(a) : a \in A\}$. Then

$$\mathbb{E}_\sigma \mathcal{R}_N(\phi \circ A) \leq L\mathbb{E}_\sigma \mathcal{R}_N A. \quad (42)$$

Appendix B. Shadow Technique

We introduce the concept of shadow following Eckstein and Nutz (2022). Let $\mu, \tilde{\mu} \in \mathcal{P}_p(\mathcal{X})$ and $\nu, \tilde{\nu} \in \mathcal{P}_p(\mathcal{Y})$. Let $\Lambda \in \Pi(\mu, \tilde{\mu})$ be a coupling attaining $W_p(\mu, \tilde{\mu})$ and $\Lambda = \mu \otimes \kappa^\mu$ be a disintegration. Similarly, let $\Lambda' \in \Pi(\nu, \tilde{\nu})$ be a coupling attaining $W_p(\nu, \tilde{\nu})$ and $\Lambda' = \nu \otimes \kappa^\nu$ be a disintegration. Denote $\kappa(x, y) := \kappa^\mu(x) \otimes \kappa^\nu(y)$. Given a coupling $\pi \in \Pi(\mu, \nu)$, its *shadow* $S(\pi)$ is the second $\mathcal{X} \times \mathcal{Y}$ marginal of $\pi \otimes \kappa \in \mathcal{P}(\mathcal{X} \times \mathcal{Y} \times \mathcal{X} \times \mathcal{Y})$. By definition, we have $S(\pi) \in \Pi(\tilde{\mu}, \tilde{\nu})$. In particular, $S(\pi)$ is also called the (κ^μ, κ^ν) -shadow of π (Eckstein and Pammer, 2023).

Lemma 31 (Eckstein and Nutz, 2022, Lemma 3.2) The coupling π and its shadow $S(\pi)$ satisfy

$$W_p(\pi, S(\pi)) = [W_p^p(\mu, \tilde{\mu}) + W_p^p(\nu, \tilde{\nu})]^{1/p}. \quad (43)$$

Proof First,

$$\begin{aligned} W_p^p(\pi, S(\pi)) &= \inf_{\gamma \in \Pi(\pi, S(\pi))} \int [d_{\mathcal{X}}^p(x, \tilde{x}) + d_{\mathcal{Y}}^p(y, \tilde{y})] d\gamma \\ &\leq \int [d_{\mathcal{X}}^p(x, \tilde{x}) + d_{\mathcal{Y}}^p(y, \tilde{y})] \pi(dx, dy) \kappa(x, y, d\tilde{x}, d\tilde{y}) \\ &= \int d_{\mathcal{X}}^p(x, \tilde{x}) \mu(dx) \kappa^\mu(x, d\tilde{x}) + \int d_{\mathcal{Y}}^p(y, \tilde{y}) \nu(dy) \kappa^\nu(y, d\tilde{y}) \\ &= W_p^p(\mu, \tilde{\mu}) + W_p^p(\nu, \tilde{\nu}). \end{aligned}$$

The last equality holds since $\mu \otimes \kappa^\mu$ and $\nu \otimes \kappa^\nu$ are optimal couplings by the definition.

For another direction, any $\gamma \in \Pi(\pi, S(\pi))$ induces two couplings $\gamma_1 \in \Pi(\mu, \tilde{\mu})$ and $\gamma_2 \in \Pi(\nu, \tilde{\nu})$. Hence,

$$\begin{aligned} W_p^p(\pi, S(\pi)) &= \inf_{\gamma \in \Pi(\pi, S(\pi))} \int [d_{\mathcal{X}}^p(x, \tilde{x}) + d_{\mathcal{Y}}^p(y, \tilde{y})] d\gamma \\ &\geq \inf_{\gamma_1 \in \Pi(\mu, \tilde{\mu})} \int d_{\mathcal{X}}^p(x, \tilde{x}) d\gamma_1 + \inf_{\gamma_2 \in \Pi(\nu, \tilde{\nu})} \int d_{\mathcal{Y}}^p(y, \tilde{y}) d\gamma_2 \\ &= W_p^p(\mu, \tilde{\mu}) + W_p^p(\nu, \tilde{\nu}). \end{aligned}$$

It proves the claim. ■

Lemma 32 *Suppose a function f satisfies*

$$\left| \int f d\pi - \int f d\tilde{\pi} \right| \leq L W_p(\pi, \tilde{\pi}), \quad \forall \pi \in \Pi(\mu, \nu), \tilde{\pi} \in \Pi(\tilde{\mu}, \tilde{\nu}), \quad (44)$$

with a constant $L > 0$. Then

$$\left| \inf_{\pi \in \Pi(\mu, \nu)} \int f d\pi - \inf_{\tilde{\pi} \in \Pi(\tilde{\mu}, \tilde{\nu})} \int f d\tilde{\pi} \right| \leq L [W_p^p(\mu, \tilde{\mu}) + W_p^p(\nu, \tilde{\nu})]^{1/p}. \quad (45)$$

Proof Denote a coupling π^* attaining $\inf_{\tilde{\pi} \in \Pi(\tilde{\mu}, \tilde{\nu})} \int f d\tilde{\pi}$. The shadow $S(\pi^*)$ of π^* is in $\Pi(\mu, \nu)$. Therefore,

$$\inf_{\pi \in \Pi(\mu, \nu)} \int f d\pi - \inf_{\tilde{\pi} \in \Pi(\tilde{\mu}, \tilde{\nu})} \int f d\tilde{\pi} \leq \int f dS(\pi^*) - \int f d\pi^* \leq L W_p(S(\pi^*), \pi^*).$$

Then we can apply Lemma 31 to obtain one side of (45). Another side follows similarly. ■

Appendix C. Properties of Sub-Root Functions

Lemma 33 (Duan et al., 2021, Lemma G.5) *Suppose $\psi(\cdot)$ is a nontrivial sub-root function and r^* is its positive fixed point, then*

- (1) *For any $C > 0$, $f(r) := C\psi(r/C)$ is sub-root and its positive fixed point r_f satisfies $r_f = Cr^*$;*
- (2) *For any $C > 0$, $f(r) := C\psi(r)$ is sub-root and its positive fixed point r_f satisfies $r_f \leq \max\{C^2, 1\} \times r^*$.*

Appendix D. Properties of Covering Number

Lemma 34 *Consider a class \mathcal{F} with a norm $\|\cdot\|$. Then $\mathcal{N}(\varepsilon, \mathcal{F} - \mathcal{F}, \|\cdot\|) \leq \mathcal{N}(\varepsilon/2, \mathcal{F}, \|\cdot\|)$, where $\mathcal{F} - \mathcal{F} := \{f_1 - f_2 : f_1, f_2 \in \mathcal{F}\}$.*

Lemma 35 *For a distribution β and constant $p \in [1, \infty)$, we have $\mathcal{N}(\varepsilon, \mathcal{F}, \|\cdot\|_{L_p(\beta_N)}) \leq \mathcal{N}_p(\varepsilon, \mathcal{F}) \leq \mathcal{N}_\infty(\varepsilon, \mathcal{F})$. Moreover, $\mathcal{N}_\infty(\varepsilon, \mathcal{F}) \leq \mathcal{N}(\varepsilon, \mathcal{F}, \|\cdot\|_\infty)$.*

Appendix E. Extension of Hölder Continuous Functions

Lemma 36 Denote a subset $A \subseteq \mathbb{R}^n$. Consider a Hölder continuous function $f : A \rightarrow \mathbb{R}$ satisfying

$$|f(x) - f(y)| \leq L|x - y|^\alpha, \quad \forall x, y \in A,$$

with some $\alpha \in (0, 1]$ and $L > 0$. Define a function g on \mathbb{R}^n as

$$g(x) := \inf_{y \in A} \{f(y) + L|x - y|^\alpha\}, \quad x \in \mathbb{R}^n. \quad (46)$$

Then $g : \mathbb{R}^n \rightarrow \mathbb{R}$ extends f in the following sense:

$$\begin{aligned} g(x) &= f(x), \quad \forall x \in A, \\ |g(x) - g(y)| &\leq L|x - y|^\alpha, \quad \forall x, y \in \mathbb{R}^n. \end{aligned}$$

Proof With $\alpha \in (0, 1]$, we will use the fact that $|a + b|^\alpha \leq (|a| + |b|)^\alpha \leq |a|^\alpha + |b|^\alpha$.

First, we show g is finite. Since f is finite and g is defined with the infimum, we only need to show $g(x) > -\infty$, $x \in \mathbb{R}^n$. Note that when $y, y' \in A$,

$$f(y) - f(y') + L|x - y|^\alpha \geq -L|y - y'|^\alpha + L|x - y|^\alpha \geq -L|x - y'|^\alpha.$$

Hence,

$$g(x) = \inf_{y \in A} \{f(y) + L|x - y|^\alpha\} \geq f(y') - L|x - y'|^\alpha > -\infty. \quad (47)$$

Then, we prove $g = f$ on A . Suppose $x \in A$. With the definition of g , we have $g(x) \leq f(x)$ by taking $y = x$ in (46). To show $g(x) \geq f(x)$, we choose $y' = x$ in (47).

Next, we show the Hölder continuity of g on \mathbb{R}^n . Given $\varepsilon > 0$, for any $x \in \mathbb{R}^n$, since g is finite, the definition of g guarantees that there exists $y \in A$ such that

$$g(x) \geq f(y) + L|x - y|^\alpha - \varepsilon.$$

Since $g(x') \leq f(y) + L|x' - y|^\alpha$ by the definition, we have

$$\begin{aligned} g(x) - g(x') &\geq f(y) + L|x - y|^\alpha - \varepsilon - f(y) - L|x' - y|^\alpha \\ &\geq -L|x' - x|^\alpha - \varepsilon. \end{aligned}$$

Let $\varepsilon \rightarrow 0$, we get $g(x) - g(x') \geq -L|x' - x|^\alpha$. Interchanging the roles of x and x' shows the Hölder continuity. ■

References

Beatrice Acciaio, Julio Backhoff-Veraguas, and Anastasiia Zalashko. Causal optimal transport and its links to enlargement of filtrations and continuous-time stochastic optimization. *Stochastic Processes and their Applications*, 130(5):2918–2953, 2020.

- Beatrice Acciaio, Julio Backhoff-Veraguas, and Junchao Jia. Cournot–Nash equilibrium and optimal transport in a dynamic setting. *SIAM Journal on Control and Optimization*, 59(3):2273–2300, 2021.
- Tobias Achterberg, Robert E Bixby, Zonghao Gu, Edward Rothberg, and Dieter Weninger. Presolve reductions in mixed integer programming. *INFORMS Journal on Computing*, 32(2):473–506, 2020.
- Erling D Andersen and Knud D Andersen. Presolving in linear programming. *Mathematical Programming*, 71:221–245, 1995.
- Martin Anthony and Peter L Bartlett. *Neural network learning: Theoretical foundations*. 1999.
- Julio Backhoff-Veraguas, Mathias Beiglbock, Yiqing Lin, and Anastasiia Zalashko. Causal transport in discrete time and applications. *SIAM Journal on Optimization*, 27(4):2528–2562, 2017.
- Julio Backhoff-Veraguas, Daniel Bartl, Mathias Beiglbock, and Manu Eder. Adapted Wasserstein distances and stability in mathematical finance. *Finance and Stochastics*, 24(3):601–632, 2020.
- Julio Backhoff-Veraguas, Daniel Bartl, Mathias Beiglbock, and Johannes Wiesel. Estimating processes in adapted Wasserstein distance. *The Annals of Applied Probability*, 32(1):529–550, 2022.
- Peter Bartlett, Olivier Bousquet, and Shahar Mendelson. Local Rademacher complexities. *Annals of Statistics*, 33(4):1497–1537, 2005.
- Vladimir I Bogachev. *Measure Theory*, volume II. Springer Science & Business Media, 2007.
- Léon Bottou and Olivier Bousquet. The tradeoffs of large scale learning. *Advances in Neural Information Processing Systems*, 20, 2007.
- Jinglin Chen and Nan Jiang. Information-theoretic considerations in batch reinforcement learning. In *International Conference on Machine Learning*, pages 1042–1051. PMLR, 2019.
- Marco Cuturi. Sinkhorn distances: Lightspeed computation of optimal transport. *Advances in Neural Information Processing Systems*, 26, 2013.
- Yaqi Duan, Chi Jin, and Zhiyuan Li. Risk bounds and Rademacher complexity in batch reinforcement learning. In *International Conference on Machine Learning*, pages 2892–2902. PMLR, 2021.
- Stephan Eckstein and Marcel Nutz. Quantitative stability of regularized optimal transport and convergence of Sinkhorn’s algorithm. *SIAM Journal on Mathematical Analysis*, 54(6):5922–5948, 2022.

- Stephan Eckstein and Gudmund Pammer. Computational methods for adapted optimal transport. *The Annals of Applied Probability*, 2023.
- Jianqing Fan, Zhaoran Wang, Yuchen Xie, and Zhuoran Yang. A theoretical analysis of deep Q-learning. In *Learning for Dynamics and Control*, pages 486–489. PMLR, 2020.
- Nicolas Fournier and Arnaud Guillin. On the rate of convergence in Wasserstein distance of the empirical measure. *Probability Theory and Related Fields*, 162(3-4):707–738, 2015.
- Aude Genevay, Marco Cuturi, Gabriel Peyré, and Francis Bach. Stochastic optimization for large-scale optimal transport. *Advances in Neural Information Processing Systems*, 29, 2016.
- Aude Genevay, Lénaïc Chizat, Francis Bach, Marco Cuturi, and Gabriel Peyré. Sample complexity of Sinkhorn divergences. In *The 22nd International Conference on Artificial Intelligence and Statistics*, pages 1574–1583. PMLR, 2019.
- Clark R Givens and Rae Michael Shortt. A class of Wasserstein metrics for probability distributions. *Michigan Mathematical Journal*, 31(2):231–240, 1984.
- Geoffrey J Gordon. Approximate solutions to Markov decision processes. *PhD thesis*, 1999.
- Bingyan Han. Distributionally robust Kalman filtering with volatility uncertainty. *arXiv preprint arXiv:2302.05993*, 2023.
- Alexander Korotin, Lingxiao Li, Aude Genevay, Justin M Solomon, Alexander Filippov, and Evgeny Burnaev. Do neural optimal transport solvers work? A continuous Wasserstein-2 benchmark. *Advances in Neural Information Processing Systems*, 34:14593–14605, 2021.
- Sophie Langer. Approximating smooth functions by deep neural networks with sigmoid activation function. *Journal of Multivariate Analysis*, 182:104696, 2021.
- Rémi Lassalle. Causal transference plans and their Monge-Kantorovich problems. *arXiv preprint arXiv:1303.6925*, 2013.
- Yunwen Lei, Lixin Ding, and Yingzhou Bi. Local Rademacher complexity bounds based on covering numbers. *Neurocomputing*, 218:320–330, 2016.
- Shahar Mendelson. A few notes on statistical learning theory. In *Advanced Lectures on Machine Learning: Machine Learning Summer School 2002 Canberra, Australia, February 11–22, 2002 Revised Lectures*, pages 1–40. Springer, 2003.
- Volodymyr Mnih, Koray Kavukcuoglu, David Silver, Andrei A Rusu, Joel Veness, Marc G Bellemare, Alex Graves, Martin Riedmiller, Andreas K Fidjeland, Georg Ostrovski, et al. Human-level control through deep reinforcement learning. *Nature*, 518(7540):529–533, 2015.
- Mehryar Mohri, Afshin Rostamizadeh, and Ameet Talwalkar. *Foundations of Machine Learning*. MIT Press, 2018.

- Rémi Munos. Error bounds for approximate policy iteration. In *International Conference on Machine Learning*, pages 560–567, 2003.
- Rémi Munos and Csaba Szepesvári. Finite-time bounds for fitted value iteration. *Journal of Machine Learning Research*, 9(5), 2008.
- Thanh Nguyen-Tang, Sunil Gupta, Hung Tran-The, and Svetha Venkatesh. Sample complexity of offline reinforcement learning with deep ReLU networks. *Transactions of Machine Learning Research*, 2022.
- Gabriel Peyré and Marco Cuturi. Computational optimal transport: With applications to data science. *Foundations and Trends® in Machine Learning*, 11(5-6):355–607, 2019.
- Georg Ch Pflug and Alois Pichler. A distance for multistage stochastic optimization models. *SIAM Journal on Optimization*, 22(1):1–23, 2012.
- Alois Pichler and Michael Weinhardt. The nested Sinkhorn divergence to learn the nested distance. *Computational Management Science*, 19(2):269–293, 2022.
- Warren B Powell. *Approximate Dynamic Programming: Solving the curses of dimensionality*, volume 703. John Wiley & Sons, 2007.
- Johannes Schmidt-Hieber. Nonparametric regression using deep neural networks with ReLU activation function. *The Annals of Statistics*, 48(4):1875 – 1897, 2020. doi: 10.1214/19-AOS1875. URL <https://doi.org/10.1214/19-AOS1875>.
- Vivien Seguy, Bharath Bhushan Damodaran, Remi Flamary, Nicolas Courty, Antoine Rolet, and Mathieu Blondel. Large-scale optimal transport and mapping estimation. In *International Conference on Learning Representations*, 2018.
- Shai Shalev-Shwartz and Shai Ben-David. *Understanding machine learning: From theory to algorithms*. Cambridge University Press, 2014.
- Taiji Suzuki. Adaptivity of deep ReLU network for learning in Besov and mixed smooth Besov spaces: optimal rate and curse of dimensionality. In *International Conference on Learning Representations*, 2019.
- Cédric Villani. *Optimal transport: old and new*, volume 338. Springer, 2009.
- Martin J Wainwright. *High-dimensional statistics: A non-asymptotic viewpoint*, volume 48. Cambridge university press, 2019.
- Tianlin Xu, Wenliang Kevin Li, Michael Munn, and Beatrice Acciaio. COT-GAN: Generating sequential data via causal optimal transport. *Advances in Neural Information Processing Systems*, 33:8798–8809, 2020.